UNIVERSIDADE DO VALE DO RIO DOS SINOS – UNISINOS

UNIDADE ACADÊMICA DE PESQUISA E PÓS-GRADUAÇÃO

PROGRAMA DE PÓS-GRADUAÇÃO EM GEOLOGIA

NÍVEL MESTRADO

DISSERTAÇÃO DE MESTRADO

Early Danian carbon cycle perturbation: calcareous nannofossil and geochemical response at Blake Nose region (ODP Site 1049C), North Atlantic

Andressa Nauter Alves

São Leopoldo

2022

Andressa Nauter Alves

Early Danian carbon cycle perturbation: calcareous nannofossil and geochemical response at Blake Nose region (ODP Site 1049C), North Atlantic

Área de Concentração: Geologia Sedimentar

Linha de Pesquisa: Paleontologia Aplicada

Tema de interesse: Micropaleontologia – Nanofósseis Calcários

Dissertação apresentada como requisito parcial para a obtenção do título de Mestre, pelo Programa de Pós-Graduação em Geologia da Universidade do Vale do Rio dos Sinos - UNISINOS

Orientador: Prof. Dr. Gerson Fauth

Coorientador: Prof. Dr. Tom Dunkley Jones (University of Birmingham/UK)

A474e Alves, Andressa Nauter.
Early Danian carbon cycle perturbation : calcareous nannofossil and geochemical response at Blake Nose region (ODP Site 1049C), North Atlantic / Andressa Nauter Alves. – 2022.
59 f. : il. ; 30 cm.

Dissertação (mestrado) – Universidade do Vale do Rio dos Sinos, Programa de Pós-Graduação em Geologia, 2022.
"Orientador: Prof. Dr. Gerson Fauth
Coorientador: Prof. Dr. Tom Dunkley Jones."

1. Geoquímica. 2. Nanofósseis. 3. Paleoceanografia. I. Título.

CDU 55

Dados Internacionais de Catalogação na Publicação (CIP)
(Bibliotecária: Silvana Dornelles Studzinski – CRB 10/2524)

Sumário

RESUMO

Excursões de isótopos de carbono (CIEs) de curta duração (10^4-10^5 anos), muitas das quais estão associadas a algum grau de aquecimento oceânico são uma característica do estado de clima quente do início do Paleogeno. A primeira dessas perturbações do ciclo de carbono do Paleogeno (evento DAN-C2: 65,80 – 65,70 Ma) foi reconhecida em testemunhos de sedimentos do oceano profundo recuperados de vários locais do Oceano Atlântico e Thethys. Embora muitos estudos tenham relatado mudanças na assembleia de foraminíferos bentônicos ao longo desse intervalo, estudos sobre a resposta de nanofósseis calcários ao longo desse evento são escassos. Aqui analisamos a distribuição de nanofósseis calcários entre 65,98 e 65,70 Ma de sedimentos de águas profundas recuperados de Blake Nose Plateau e combinamos esses resultados com dados geoquímicos (fluorescência de raios X, carbonato de cálcio, carbono orgânico total e conteúdo de mercúrio) para entender as principais mudanças paleoabientais ao longo deste evento. De 65,98 a 65,80 Ma a produtividade oceânica superficial estava alta, dominada principalmente por espécies de Futyania petalosa. As relações Fe/K indicam condições climáticas áridas. O aumento das razões Hg/TOC (ppb/%) e Hg/Al (ppb/cps) registrado em 65,90 Ma sugere fortemente que a atividade vulcânica, provavelmente relacionada ao vulcanismo Deccan (Índia), precedeu o evento DAN-C2. Este achado está associado a um aumento no teor de carbonato de cálcio (CaCO3 %) e na produção biogênica (Ca/Fe), levando a uma melhora na preservação dos nanofósseis calcários. No início do DAN-C2 (65,80 Ma), o índice de diversidade de Shannon (H) mostra aumento da diversidade de espécies de nanofósseis, com maior abundância de espécies eutróficas e de alta fertilidade. Intemperismo mais intenso e escoamento de nutrientes provavelmente impulsionaram essas condições durante o evento. Além disso, fornecemos novas evidências de que nanofósseis calcários (*Coccolithus pelagicus* e *Cruciplacolithus*

primus) reduziram o tamanho ao longo do evento DAN-C2, em um intervalo de intensa dissolução e sequestro de dióxido de carbono. Finalmente, sugerimos que a dinâmica das correntes oceânicas de superfície é um mecanismo importante para explicar a excursão negativa mais forte de $\delta^{13}C$ observada em Blake Nose. O ciclo máximo de excentricidade provavelmente amplificou os efeitos de níveis de CO_2 semelhantes aos atuais, levando a mudanças locais na paleocirculação combinada com remobilizações de sedimentos do Golfo do México e aumentando o sequestro de CO_2 para sedimentos oceânicos profundos.

1. APRESENTAÇÃO

1.1. Introdução

Os Nanofósseis Calcários são classificados como todos os fósseis de composição calcária menores que 63 microns (μm), com exceção a fragmentos ou formas juvenis de fósseis maiores como foraminíferos (Segundo terminologia da Associação Internacional de Nanofósseis). Esse grupo é dividido em duas categorias, os cocólitos e as formas associadas. Os cocólitos possuem formas elípticas a circulares e provém da desagregação do envoltório carbonático de algas unicelulares. As formas associadas exibem estruturas com maior variabilidade, não sendo definidas taxonomicamente (incertae sedis) devido à falta de análogos vivos, essas formas são conhecidas como nanolitos (Bown and Young, 1998). As algas unicelulares, conhecidas como cocolitoforídeos, possuem hábito marinho e tem sua distribuição vertical e horizontal na coluna d'água controlada por condições ecológicas, bem como: nutrientes, salinidade, temperatura, disposição de luz, vitaminas e minerais (Winter et al., 1994).

O intervalo de tempo Paleoceno é considerado uma época de rápida evolução para nanofósseis calcários logo após a grande extinção do limite Cretáceo– Paleogeno (K/Pg), que ocasionou uma perda de cerca de 93% das assembleias de nanofósseis do Cretáceo Superior, as primeiras formas cenozoicas são caracterizadas pelo tamanho inicialmente

diminuto (aprox. 2µm) e pela morfologia distinta das formas Mesozoicas (Bown, 2005). Além disso, diversos eventos de rápido aquecimento são documentados durante esse intervalo, denominados como “Hipertermais”, esses episódios são reconhecidos como intervalos de elevada concentração de gases de efeito estufa (Greenhouse) na atmosfera (e.g. Quillévéré et al., 2008; Westerhold et al., 2011; Zachos et al., 2010). O primeiro evento de rápido aquecimento é conhecido como DAN-C2, que tem seu registro no início do Daniano. Esse intervalo tem sido estudado por diferentes autores (e.g. Coccioni et al., 2010; Krahl et al., 2020; Quillévéré et al., 2008; Barnet et al., 2019; Palcu et al., 2020) posicionando o evento dentro da magnetozona C29r.

As assinaturas geoquímicas nas regiões registram uma queda dupla na razão isotópica ($^{13}C/^{12}C$), caracterizando uma excursão negativa de carbono (CIE) reconhecida tanto em sedimento e em planctônicos e bentônicos, já os indicadores de paleotemperatura ($^{18}O/^{16}O$), quando analisado em sedimento e em foraminíferos planctônicos indicam aquecimento das águas superficiais (~ 4°C) (Quillévéré et al., 2008). Ademais, esse intervalo é caracterizado por dissolução de carbonato de cálcio concomitante com aumento de susceptibilidade magnética dos sedimentos (e.g. Quillévéré et al., 2008; Coccioni et al., 2010) (Figura 1).

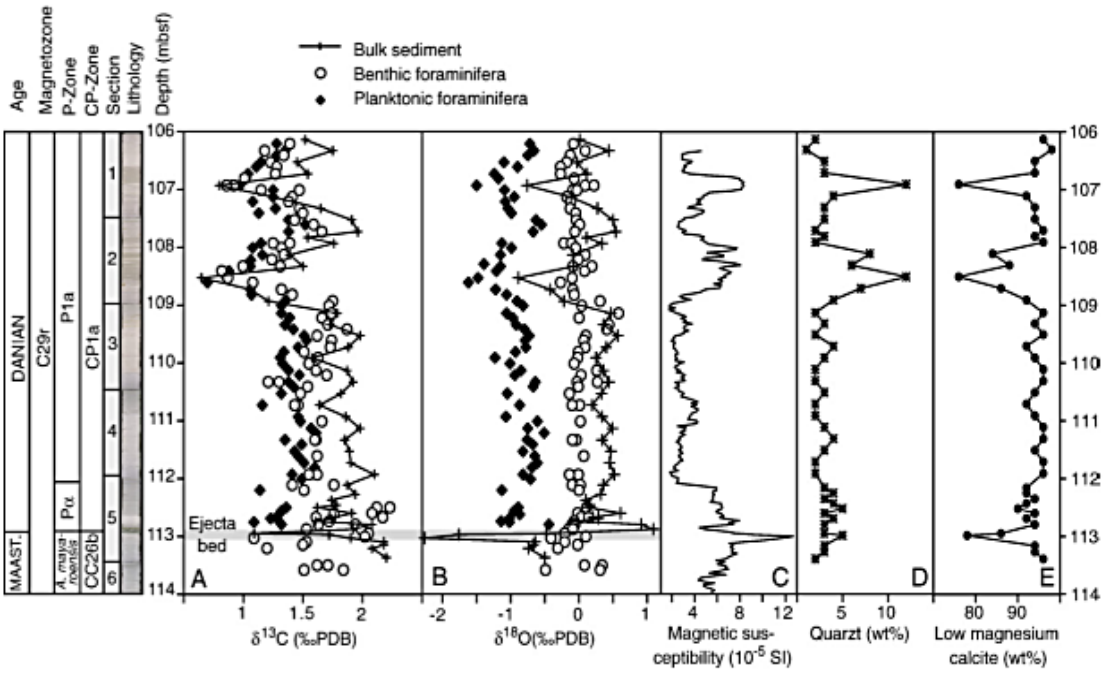

Figura 1. Variações em $\delta^{13}C$ (A) e $\delta^{18}O$ (B) dos sedimentos, foraminíferos planctônicos e bentônicos durante o início do Daniano para o *Site* ODP 1049C. Dados de suscetibilidade magnética (C) de acordo com Norris et al. (1998). Correlações mineralógicas, quartzo (D) e calcita de baixo-magnésio (E) segundo Speed e Kroon (2000). Figura extraída de Quillévéré et al. (2008).

1.2. Área de estudo

Para a presente dissertação foram escolhidas amostras da região do Atlântico Norte ODP 1049 *Hole* C. O *Site* 1049C (30°8.5370´N, 76°06.7271'W) é localizado na margem mais a leste da escarpa Blake, na região denominada Blake Nose, no oeste do Atlântico Norte sob uma lâmina d'água de 2671m (Norris et al., 1998). No início do Daniano ambos a região estava localizada em uma zona subtropical ~ 25°N (Site 1049C; Ogg et al., 2001). Esse site foi definido por apresentar uma paleoprofundidade rasa comparada a outras regiões (1500 – 1600 m) (Alegret and Thomas, 2004), garantindo uma deposição acima da zona de compensação do carbonato de cálcio

(CCD), e também por apresentar maior magnitude de queda na razão isotópica $^{13}C/^{12}C$ (~ 1,2 ‰) reconhecida em sedimentos (Quillévéré et al., 2008).

1.3. Objetivos

O objetivo geral desse projeto é compreender quais efeitos podem ser observados nas assembleias de nanofósseis calcários durante esse intervalo de instabilidade paleoambiental no início do Daniano, associado a excursão negativa de carbono (evento DAN-C2) na região de Blake Nose (*Site* ODP 1049C). Seguindo os objetivos específicos listados abaixo:

i. Avaliar as condições paleoambientais e os sinais geoquímicos durante o evento DAN-C2 nas áreas selecionadas

ii. Analisar a morfologia e os efeitos de preservação nas assembleias de nanofósseis calcários.

1.4. Justificativa

Estudos recentes vêm questionando o papel do vulcanismo do Deccan (Índia) durante esse intervalo (Gilabert et al., 2021) e a falta de indicadores robustos para aquecimento superficial dos oceanos (Arreguín-Rodríguez et al., 2021). Além disso, as excursões negativas de isótopo de carbono (CIE) e os processos envolvidos ainda são intensamente debatidos pela comunidade científica.

Nanofósseis calcários tem um papel fundamental dentro do ciclo do carbono, sendo que mudanças na distribuição das assembleias respondem a variações em outras esferas. Estudos voltados para mudanças paleoecológicas com base em nanofósseis calcários são consideravelmente escassos durante o evento DAN-C2, e podem corroborar para a caracterização desse evento no Atlântico Norte.

1.5. Hipótese

A análise do padrão de distribuição e parâmetros preservacionais das assembleias de nanofósseis juntamente com as variações geoquímicas ocorridas na coluna d'água nesse intervalo, podem corroborar para um melhor entendimento acerca das mudanças

paleoambientais envolvidas e os efeitos na biota marinha durante o DAN-C2 na região de estudo.

1.6. Metodologia

Para atingir os objetivos, foram aplicadas análises geoquímicas (Fluorescência de raio x e concentrações de carbonato de cálcio, carbono orgânico total e mercúrio) e análises do padrão de distribuição dos nanofósseis calcários nas amostras coletadas (contagem de espécies por amostra, análise de preservação com uso de Microscópico Eletrônico de Varredura, e medidas morfométricas das espécies selecionadas). Toda metodologia aplicada nesse estudo é detalhada ao longo do artigo.

Os resultados obtidos serão apresentados no capítulo 1 deste trabalho em formato de artigo científico em inglês e nas normas da revista ao qual foi submetido (Global and Planetary Change) - Qualis A2. As figuras estão citadas no texto e apresentadas ao longo do artigo. Por fim, no Capítulo II será apresentada uma síntese integradora de toda dissertação de Mestrado.

I. MANUSCRIPT

Biotic turnover and carbon cycle dynamics in the early Danian event (Dan-C2): new insights from Blake Nose, North Atlantic

Andressa Nauter-Alves[a,b], Tom Dunkley Jones[c], Mauro Daniel Rodrigues Bruno[a,b], Marcelo A. De Lira Mota[b], Guilherme Krahl[a,b], Gerson Fauth[a,b]

[a] Post-Graduate Program in Geology, Universidade do Vale do Rio dos Sinos- Unisinos University, São Leopoldo, Rio Grande do Sul, Brazil

[b] Itt Oceaneon – Instituto Tecnológico de Paleoceanografia e Mudanças Climáticas, Unisinos University, São Leopoldo, Rio Grande do Sul, Brazil

[c]School of Geography, Earth and Environmental Sciences, Birmingham University, Birmingham, UK

Abstract

Short-lived (10^4-10^5 years) carbon isotope excursions (CIEs), many of which are associated with some degree of ocean warming, are a feature of the warm climate state of the early Paleogene. The first of these Paleogene carbon cycle perturbations (DAN-C2 event: 65.80 – 65.70 Ma) has been recognized in deep-ocean sediment cores recovered from a number of Atlantic Ocean and Thethys locations. Although many studies have reported benthic foraminifera assemblage changes across this interval, studies of the calcareous nannofossil response across this event are scarce. Here we analyse the distribution of calcareous nannofossils between 65.98 and 65.70 Ma from deep-sea sediments recovered from Blake Nose Plateau and combine these results with geochemical data (X-ray fluorescence, calcium carbonate, total organic carbon, and mercury content) to understand the main palaeoecological changes across this event. From 65.98 to 65.80 Ma surface ocean productivity was high, mainly dominated by *Futyania petalosa* species. Fe/K ratios indicate arid climate conditions. Increased Hg/TOC $_{(ppb/\%)}$ and Hg/Al $_{(ppb/cps)}$ ratios recorded at 65.90 Ma strongly suggest that volcanic activity, likely related to the Deccan Traps, preceded the DAN-C2 event. This

finding is associated with an increase in calcium carbonate content ($CaCO_3$ %) and biogenic production (Ca/Fe), leading to an improvement in calcareous nanoplankton preservation. At the onset of DAN-C2 (65.80 Ma), Shannon diversity (H) index shows increased nannofossil species diversity, with greater abundances of eutrophic and high fertility species. More intense weathering and nutrient runoff most likely drove this during the event. Additionally, we provide new evidence that calcareous nannofossils (*Coccolithus pelagicus* and *Cruciplacolithus primus*) reduced size across DAN-C2 event, in an interval of intense dissolution and carbon dioxide sequestration. Finally, we suggest that surface ocean currents dynamics are an important mechanism to explain the strongest $\delta^{13}C$ negative excursion observed in Blake Nose. Eccentricity maxima cycle likely amplified the effects of similar-to-today CO_2 levels, leading to local changes in paleo circulation combined with sediments remobilizations from Gulf of Mexico, and enhance CO_2 drawdown to deep ocean sediments.

Keywords: DAN-C2 event; Site ODP 1049C; Deccan Traps; carbon excursion; calcareous nannofossils; reducing coccolith size.

1. Introduction

The early Paleocene is a time of recovery, for both ecosystems and global biogeochemistry, following the Cretaceous – Paleogene mass extinction (K/Pg: 66.001 Ma; Dinarès-Turell et al., 2014) (e.g. D'Hondt, 2005; Hull and Norris, 2011). The proximal cause of the big extinction was the Chicxulub bolide impact (e.g. Hull et al., 2020), although the effect of Deccan Traps volcanism on ecosystems and climate is still debated (e.g. Courtillot et al., 1988; Font et al., 2016; Petersen et al., 2016; Keller et al., 2020), due to pulses of volcanic eruption in the latest Maastrichtian and early Danian (Schoene et al., 2019; Sprain et al., 2019). A great impact is documented in marine realm with several generic extinction levels, all among plankton, sponges, brachiopods,

mollusks, and marine reptile's groups (e.g., Sepkoski, 1996; Racki, 2021). Marine calcareous phytoplankton (coccolithophores) show a significantly higher level of extinction with > 90 % of Maastrichtian species not surviving to the early Danian (Bown, 2005). This species loss was likely a key driver of a decline in both organic carbon and calcium carbonate flux to the deep sea that is documented around the world (e.g., Zachos et al., 1989; D'Hondt, 2005, 1998). The return to normal oceanographic conditions and marine primary production has been extensively debated, with significant geographic variations (Hull and Norris, 2011; Rosenberg et al., 2021). The Paleocene is also featured by a series of carbon isotope excursions (CIEs), which are associated with short episodes of ocean warming (e.g., Barnet et al., 2019). Most of these short-lived warming events have been associated with maxima in the 405-kyr eccentricity cycle (Zachos et al., 2010; Barnet et al., 2019; Westerhold et al., 2020; Gilabert et al., 2021), with the exception of the Paleocene – Eocene Thermal Maximum (PETM, approx. 55.5 Ma) (e.g. Zachos et al., 2010).

The earliest Paleocene CIE is the Danian DAN-C2 event, starting at 65.80 Ma with a duration of ~ 100 kyr (Quillévéré et al., 2008). The DAN-C2 event has been recognized in sediments from many different sites (Fig. 1), including ocean drilling sites in the Atlantic Ocean (Quillévéré et al., 2008; Krahl et al., 2020; Arreguín-Rodríguez et al., 2021), marine continental margin successions from Spain (Gilabert et al., 2021) and Gubbio, Italy (Coccioni et al., 2010), as well as continental settings, Ukraine (Gilmour et al., 2013). In existing records, the DAN-C2 event is often characterized by double negative excursions in carbon isotopes ratios ($\delta^{13}C$) from planktonic and benthic foraminifera, and bulk sediments at the top of magnetochron C29r, transient warming (~4°C) as recorded by $\delta^{18}O$ of planktonic foraminifera, and deep-ocean carbonate dissolution often seen as an increase in magnetic susceptibility of sediments (Quillévéré

et al., 2008; Coccioni et al., 2010; Gilmour et al., 2013; Krahl et al., 2020; Arreguín-Rodríguez et al., 2021; Gilabert et al., 2021). Geochemical data of redox condition elements and benthic foraminifera assemblages also indicate a decline in water column oxygenation at this time (Quillévéré et al., 2008; Coccioni et al., 2010; Krahl et al., 2020). Previous studies have associated the injection of light carbon into the ocean a response to Deccan Traps volcanism and orbital forcing (Quillévéré et al., 2008; Coccioni et al., 2010; Gilmour et al., 2013; Krahl et al., 2020). On the other hand, recent studies have questioned the role of volcanism injections across DAN-C2 event (Gilabert et al., 2021), and the lack of global surface warming temperatures in the interval (Arreguín-Rodríguez et al., 2021). Besides that, the majority of studies across DAN-C2 interval are related to geochemistry and benthic foraminiferal assemblages, the calcareous nannofossils response is only known from the Gubbio section, Italy (Coccioni et al., 2010), and a low resolution study from Shatsky Rise, Pacific Ocean (Ocean Drilling Program – ODP Site 1209) (Alvarez et al., 2019). Calcareous nannofossils have a key role in carbon and calcium carbonate flux to deep ocean through biological pump, thus, changes in their distribution have direct impact in global biogeochemical cycle (Falkowski, 1998).

Here, we study the ODP Site 1049C, Blake Nose, North Atlantic. We selected this site due to its shallow location during K/Pg (~1500 m), which guarantee a deposition above Carbonate Compensation Zone (CCD) at that time. Furthermore, this site presents the most expressive carbon isotope excursion (~ 1.3 ‰) when compared to other section. The aims of this study are to analyse the calcareous nannofossil response during DAN-C2 event, considering their paleoecology, preservation, and morphology. We also combined different geochemical techniques (X-ray fluorescence, calcium carbonate content, total organic carbon, and mercury concentrations) to better understand the

major changes in carbon cycle across this event. Our data provide new insights into volcanic activity across DAN-C2 and its impact on primary producers at the Blake Nose region.

2. Material and methods

2.1 Geological setting

ODP Site 1049C is located at the eastern margin of Blake Nose Plateau, western North Atlantic Ocean (30°8.5370′N, 76°06.7271’W, 2671 meters below sea level (mbsl) (Norris et al., 1998). The Site was positioned at a latitude of ~25°N (Ogg and Bardot, 2001) during early Danian (Fig. 1). Although early studies have been assigned a paleodepth of ~2500 m for this site during this interval (e.g. Frank and Arthur, 1999), benthic foraminiferal results have suggested a shallow deposition (1500-1600 m, lower bathyal) (Alegret and Thomas, 2004). The sediments are composed of a pale greenish-grey, clayey calcareous nannofossil ooze (Norris et al., 1998).

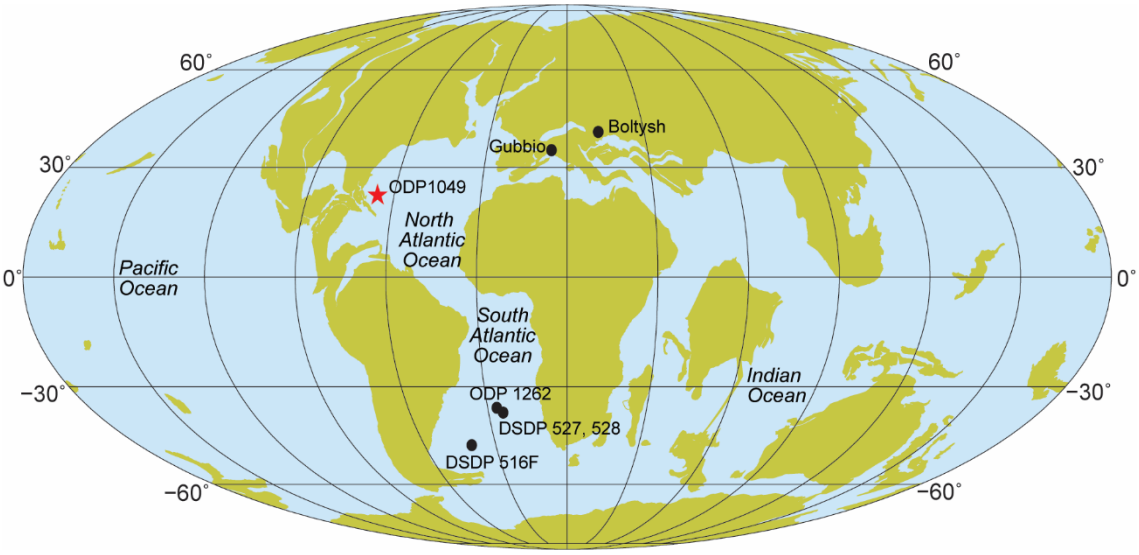

Figure 1. Paleogeographic reconstruction at the K/Pg boundary (ODSN system: http://www.odsn.de/odsn/services/ paleomap/paleomap.html). The study section ODP site 1049 (red star) and all other sites discussed in the text (black dots) are shown.

2.2. Biostratigraphic framework and age-depth model

Previous age model for ODP Site 1049C was based on the Geological Time Scale (GTS, 2004) (Quillévéré et al., 2008). We applied the updated astrochronology calibration for the Danian (Dinarès-Turell et al., 2014) to obtain a more accurate age for our results. Three tie points throughout the section yielded an age-depth model: the K/Pg boundary (113.0 m), magnetochron C29r/C29n (106.63 m), and C28r/C28n (105.83 m). Besides that, we were unable to record the C29n/C28r boundary from report section (Ogg and Bardot, 2001), and this magnetochron was not considered in our age-depth model. Based on the age-depth model generated, we inferred the DAN-C2 age between 65.80 and 65.70 Ma (Fig. 2), which is in accordance with new studies in South Atlantic sites (Barnet et al., 2019; Krahl et al., 2020; Arreguín-Rodríguez et al., 2021) and Zumaia sections (Gilabert et al., 2021).

We also applied the Calcareous Nannofossil Paleocene codes (CNP zonation scheme) to the interval, this biostratigraphical zonation is recommended for low and middle latitudes (Agnini et al., 2014). Although, previous studies had positioned the section within CP1a (Okada, H.; Bukry, 1980) calcareous nannofossil zonation (Norris et al., 1998; Quillévéré et al., 2008). This zonation scheme is no longer used for biostratigraphy in this interval of study.

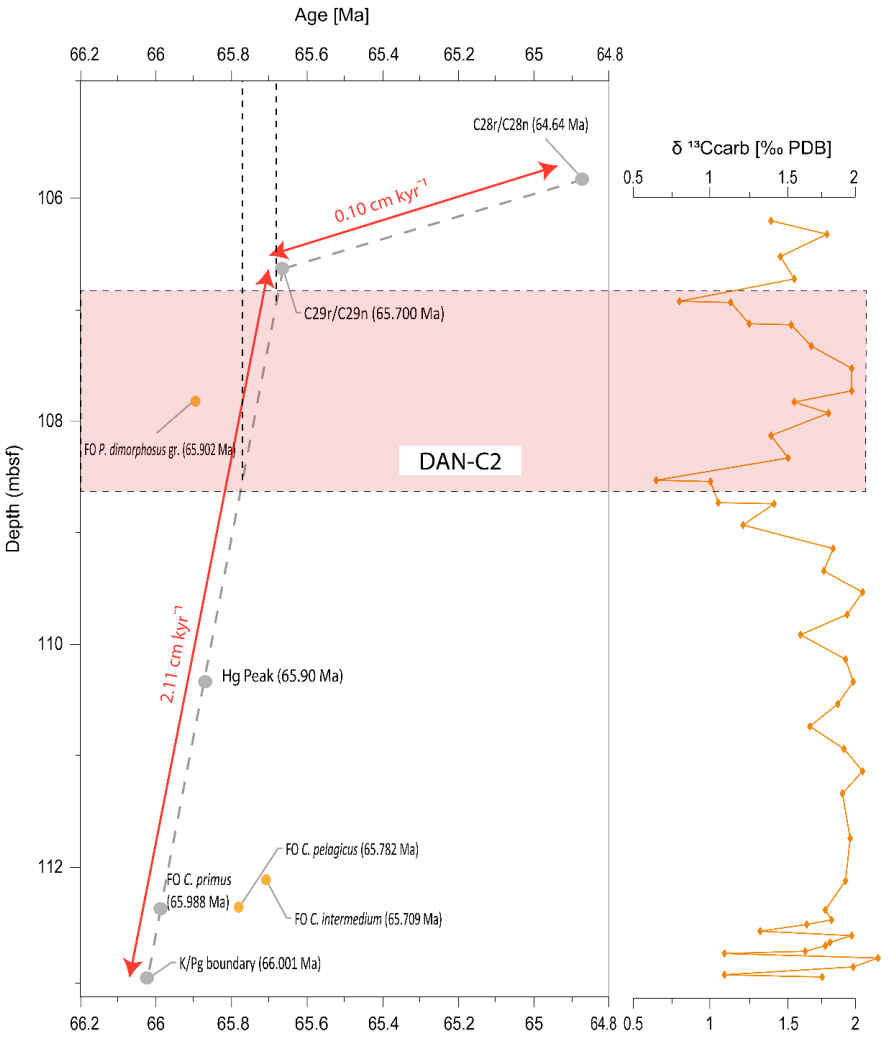

Fig. 2. Age-depth model for ODP Site 1049C and respectively tie points applied (grey dots), and its correlation with $\delta^{13}C$ (Quillévéré et al., 2008). Time scale based on Dinarès-Turell et al. (2014), stablishing DAN-C2 ages from 65.8 to 65.7 Ma. The sedimentation rate is defined in red and outlier's species in yellow dots.

2.3. Methods

Samples (n = 34) were selected with a stratigraphic resolution of ~20 cm (from 112.37 m to 106.15 m) (Fig. 3). The material was prepared for calcareous nannofossils and geochemical analyses, as summarized in the following sections.

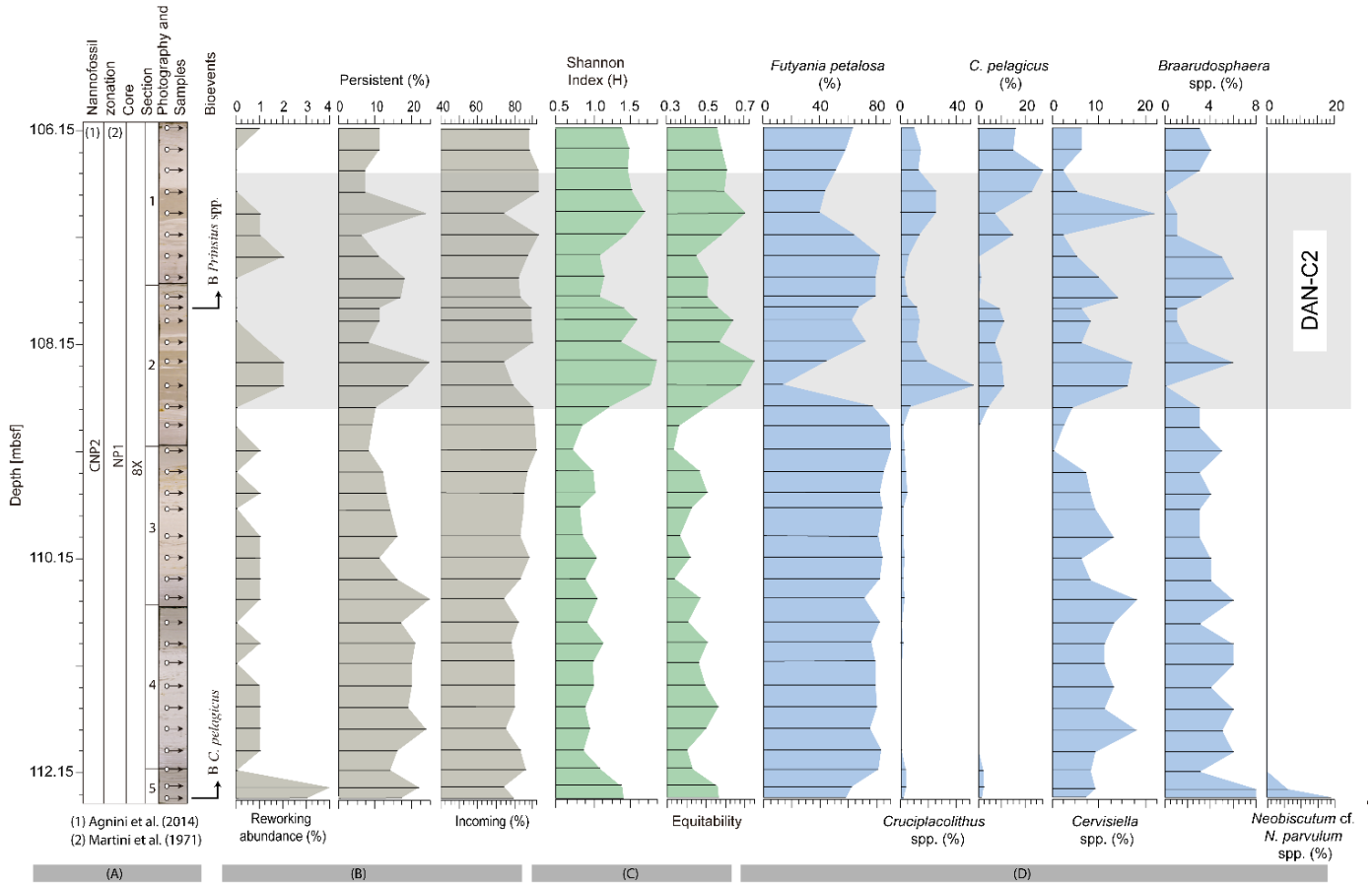

Fig. 3. A) Section profile with depth (core photography from Norris et al., 1998), all the samples analysed here are marked by an arrow. Nannofossils zonation follows biohorizons from Agnini et al. (2014). B) Percentage of Reworking, persistent, and incoming species from Danian. C) Shannon index (H) and equitability (E); D) Abundances (%) of main calcareous nannofossils discussed in this study.

2.3.1. Calcareous nannofossils

Calcareous nannofossil samples were prepared using standard smear slide techniques (Bown and Young, 1998). Samples were examined on a Zeiss Axio imager A2 microscope at 1000x magnification. The smear slides are stored in the collection of the Museum of Geological History of Rio Grande do Sul, Unisinos University, Brazil, under the curatorial numbers ULVG 13437 to ULVG 13470.

Regarding relative abundance, at least 400 specimens were counted and when necessary, the counting was extended until all specimens in the field of view (FOV) were considered in the counts (Appendix A). We considered *Cervisiella* spp. fragments larger than 4 μm as a single specimen (Following, Coccioni et al., 2010). We counted individuals *Futyania petalosa*, however, when the specimens were agglomerated (> 4 specimens), we included them as a single organism due to the high abundance of this species.

Shannon diversity (H) and Equitability (E) were calculated through Paleontological Statistic software package (PAST) (v. 4.07; Hammer et al., 2001). Shannon diversity (H) is used to evaluate biodiversity through the number of species and the equitability of their distribution in the sample (Holbourn et al., 1999). The Equitability index (E) is the degree of dominance in the assemblage and is calculated by the division of the Shannon index by the natural log of the number of species.

Morphometric analyses of *C. primus* and *C. pelagicus* were undertaken on 15 samples between 108.74 to 106.15 m. The minimum and maximum length of 100 randomly selected placoliths were measured for each sample and each species (O'Dea et al., 2014), from which the average (±1σ) and median of both measures (maximum and minimum length were calculated (Appendix B and C). These species were selected due to their high abundance through the top of the section and because some authors have

recently documented variations in the size of these species as an ecological response in a stressed environment (Narciso et al., 2006; O'Dea et al., 2014; Thibault et al., 2018). These species are rare from 112.37 to 108.92 m and so this interval was not considered for morphometric analysis. Low abundance of *C. primus* was documented at 107.34 m and only 19 specimens were measured in this sample. *Coccolithus pelagicus* was not recorded in three samples (107.52, 107.54, and 107.34 m), and its low abundance was registered at 108.74 m, where 41 specimens were measured. Additionally, frequency and boxplot distribution for each sample, as well as linear correlation of all the measures ($N_{(total)}$ = 1319 for *C. primus* and 1141 for *C. pelagicus*) are reported in section 3.1.2.

For preservation analysis, three samples (110.14, 108.54, 106.54 m) were selected for Scanning Electron Microscope observation (SEM). For each of these samples ~0.5 g of sediment was gently crushed and suspended in 40 ml of deionized water. This solution was ultrasonicated for 15 s, three times. Six drops of the concentrated solution were diluted into 200 ml of deionised water, which was then filtered through a 47 mm diameter, 3 μm pore-size Millipore filter (adapted from Okada, 2000). The filter was glued to a SEM stub and coated with a gold target and placed in an SEM – EVO MA 15 Zeiss at Itt Oceaneon.

2.3.2. Calcium carbonate and Total organic carbon

$CaCO_3$ and total organic carbon (TOC) contents were measured using 1 g of bulk sediment. Samples were homogenised, acidified with HCl (6N) (1:1) for 24 h, and washed with distilled H_2O until it reached a neutral pH. Analyses were performed at Itt Oceaneon in a LECO, SC-144DR carbon analyser with combustion temperature set to 1350 °C. The concentrations are presented as weight per cent (%).

2.3.3. X-Ray fluorescence analyses (XRF)

XRF was performed to examine major and trace elements present in bulk samples. All 34 samples were processed following the methodology described in Krahl et al. (2020) and analysed at Itt Oceaneon in an Epsilon 1/PANalytical XRF spectrometer. The results are presented in counts per second (cps). Furthermore, we applied geochemical elements based in Hughes et al. (2015) review, all the proxies used here have been applied in sediments core from marine settings, which reflect the similar conditions found in Site 1049C.

Iron/potassium ratio (Fe/K) was used here to identify periods of enhanced humidity/aridity (Moreno et al., 2006; Mulitza et al., 2008). Potassium/titanium (K/Ti) ratio was employed for weathering intensity and erosion (Schütz and Rahn, 1982; Arnaud et al., 2012; Degeai et al., 2018). Additionally, we applied terrigenous elements/calcium ratio to assess the carbonate and biogenic production, which is represented by Al+Si+K+Ti+Fe/Ca and the Ca/Fe ratios (Peterson et al., 2000; Beil et al., 2018).

2.3.4. Multivariate statistics

Cluster analysis using the program PAST (v. 4.07; Hammer et al., 2001) was performed to identify similarities between XRF proxies (Fe/K, K/Ti, Terr/Ca, and Fe/Ca), as well as the $CaCO_3$ and TOC contents. The coefficient of Euclidean distance and the UPGMA strategy (Unweighted Pair Group Method using Arithmetic Averages) was used considering a data matrix including the different geochemical data per sample (Appendix D).

2.3.5. Mercury concentration (Hg)

Hg concentrations, which have been used to identify phases of enhanced volcanic-derived inputs to sediments (e.g. Shen et al., 2020), were measured in 31 samples (from

111.93 to 106.15 m). These analyses were performed at itt Oceaneon in a direct mercury analyser (DMA-80 evo tricell double beam), following the protocol: ~0.05 g of sediment was weighed into a nickel combustion boat and placed in an autosampler. Samples were dried and thermally decomposed, with Hg vapor captured in a gold amalgamator and then released at 850 °C, to be quantified by atomic absorption spectroscopy at 254 nm. Hg results are presented in ppb and normalized to TOC (%) and Al (cps) (Appendix D), to account for organic and detrital host phases as recommended in Shen et al. (2020).

3. Results

3.1. Calcareous nannofossil assemblages

The presence of *C. pelagicus*, whose base (B) defines the base of CNP2, is recorded from 112.37 m to 106.15 m, placing the section in the CNP2 biozone of Agnini et al., (2014). We did not recover the top of CNP2, which is defined by the base common (BC) *Praeprinsius dimorphosus* group, as the abundance of this species is consistently low in the section.

We recognized eighty species (52 from Cretaceous and 28 from Cenozoic, which is included persistent and incoming species) through the section. Incoming species are the most relevant in the section with an average of 84 %, whereas the persistent show an average of 15 %. Reworked species are the least representative with an average of 1 %, although, from 112.37 to 112.27 m their percentage is slightly higher (3-4 %) (Fig. 3).

The species richness of incoming taxa is low, ranging from 10 (111.53 m) to 21 species (108.32 m). A semi-quantitative assessment of calcareous nannofossil abundance can be made from the number of nannofossils per field of view, which varies from ~7 (106.94 m) to high values of ~$144_{(N/FOV)}$ (111.33 m) (Appendix A). Shannon and Equitability indexes (Fig. 3) remain low from 112.37 to 108.74 m with an average

of 1.01 (H) and 0.46 (E), followed by an increase to average values of 1.50 (H) and 0.58 (E) from 108.54 to 106.15 m.

Relative abundance trends and species discussed here are shown in Fig. 3 and Fig. 4, other species present in lower abundance (1-3 %) were excluded from paleoecological interpretations, although all abundances are given in Appendix A.

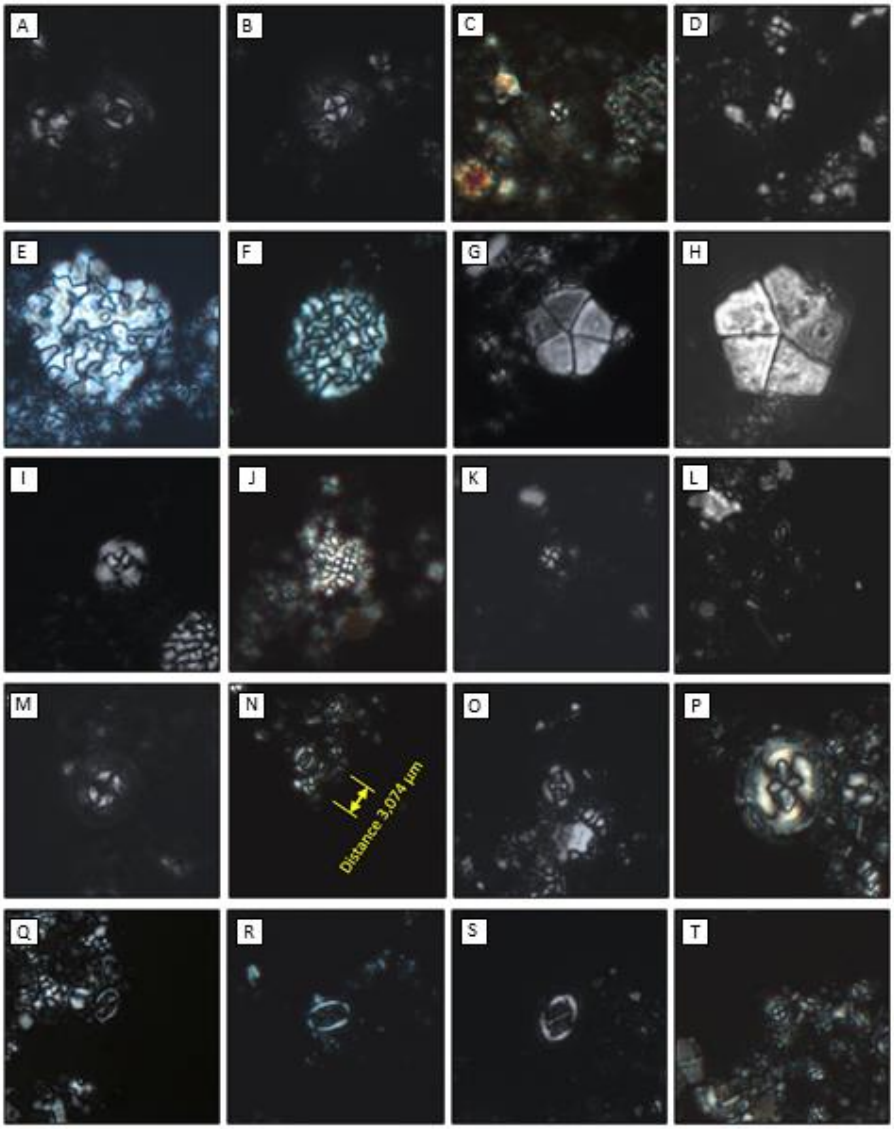

Figure 4. Calcareous nannofossils recognized at the Blake Nose section. Pictures are taken under cross-polarized light at 1000 × magnification. A) *Markalius apertus*; B) *Markalius inversus*; C) *Markalius walvisensis*; D) *Octolithus multiplus*; E) *Cervisiella saxea*; F) *Cervisiella operculata*; G) *Braarudosphaera* cf. *B. bigelowii*; H)

Braarudosphaera bigelowii; I) *Cyclagelosphaera alta*; J-K) *Futyania petalosa*; L) *Neobiscutum cf. N. parvulum*; M) *Coccolithus pelagicus*; N) *Cruciplacolithus primus* (<5 µm); O) *Cruciplacolithus primus* (<7 µm); P) *Cruciplacolithus intermedius* (>7 µm); Q) *Neochiastozygus denticulatus*; R) *Neochiastozygus digitosus*; S) *Neochiastozygus* sp 1.; T) *Prinsius* cf. *P. tenuiculus*.

Futyania petalosa is the dominant taxon, as its abundance varies from 13 % (Sample 108.54 m) to 90 % (109.14 m), followed by *Cruciplacolithus* spp., which has low abundance in some samples (1-4 %, from 112.37 to 108.92 m) but becomes more common above 108.74 m, reaching 53 % of total abundance at 108.54 m, before declining again to 2 % at 107.54 m. This genus comprises the counts of *C. primus* small (< 5 µm), *C. primus* large (< 7 µm), and *C. intermedius* (> 7 µm) (see classification of Thibault et al., 2018). *Cocccolithus pelagicus* is the third most abundant taxa, although its percentage is low (1-2 %) from 112.37 to 112.11 m, and rare with only presence logged outside of the counts from 111.93 to 108.92 m. The overall abundance of this species increases above 108.74 m, reaching 28 % at 106.54 m, with a slight decline from 107.72 to 107.34 m.

Another common genus is *Cervisiella* spp., comprising *C. operculata* and *C. saxea*, with relative abundance from 2 % (108.92, 107.14, 106.54 m) to 22 % (106.94 m). *Neobiscutum* specimens are classified here as *Neobiscutum* cf. *N. parvulum*, despite the size of specimens (< 2 µm), which could prevent a clear taxonomic classification of the genus *Neobiscutum*, we identified *N.* cf. *N. parvulum* on the basis of a birefringent tube cycle and narrow central area, allowing us to distinguish it from *N. romeini.* This species is present at 112.37 m (19 %) and 112.27 m (6 %).

Braarudosphaera spp. is less abundant with percentages varying from 1 % (107.94, 107.8, 107.14, 106.94 m) to 8 % (112.37 to 112.27 m), and rare occurrence at 108.54 and 106.74 m with only 1-2 occurrences. This genus includes *Braarudosphaera bigelowii* and *Braarudosphaera* cf. *B. bigelowii*, the latter is similar to the former but with more rounded pentaliths.

3.1.1. Preservation aspects

The three samples selected for SEM imaging represent Pre-CIE (110.14 m), the CIE onset (108.54 m), and the recovery phase after second $\delta^{13}C$ negative spike (106.54 m) (Fig. 5). Calcareous nannofossil assemblages prior to and after the DAN-C2 event show moderate to good preservation, coccoliths are slightly dissolved with delicate structures such as inner crosses partially intact but with low signs of overgrown (Fig. 5A-C; G-I). High levels of dissolution are present at the onset of the event (108.54 m), where we recorded calcareous nannofossil assemblages with no delicate structures preserved and high levels of fragmentation within clay-rich sediments. High level of dissolution and overgrown limited species classification (Fig. 5D-F).

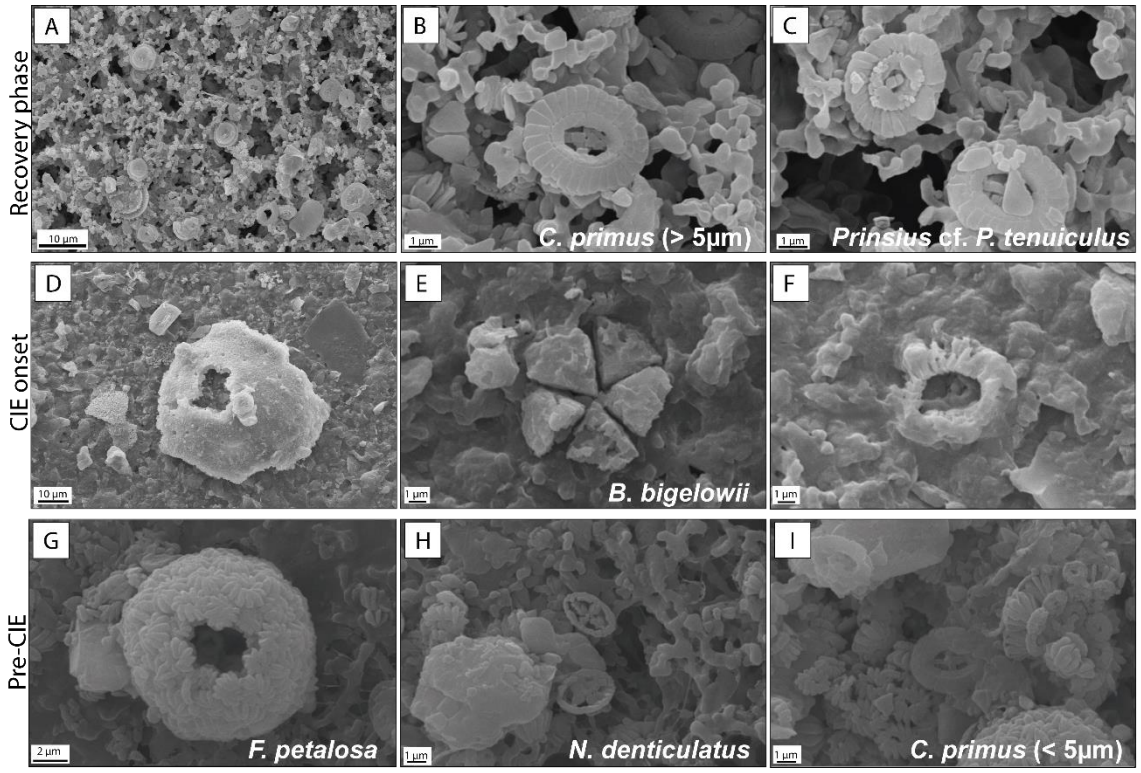

Figure 5. SEM images from selected samples at site ODP 1049C. A-C) Moderate to good assemblage preservation, sample 8X-1, 44-46 cm (106.54 m); D-F) High levels of dissolution with delicate structures dissolved, sample 8X-2, 94-96 cm (18.54 m); G-I) Good preservation signals with small and delicate inner structures preserved, sample 8X3-104-106 cm (110.14 m).

3.1.2. Size evolution of Cruciplacolithus primus and Coccolithus pelagicus

Cross plot of coccolith width versus length for both *C. primus* and *C. pelagicus* show strong linear correlations, (*C. primus* $R^2 = 0.85$, Fig. 5A; *C. pelagicus* $R^2 = 0.75$, Fig. 5B). *Cruciplacolithus primus* length varies from 2.01 to 6.99 µm with a median value of 4.37 µm, and high frequencies around 4.2 µm correlating with the small morphotype (< 5 µm) (Fig. 5A). The size distribution of *C. pelagicus* varies from 2.30 to 8.44 µm with a median of 4.43 µm and highest frequencies from 4.06 to 5.09 µm (Fig. 5B).

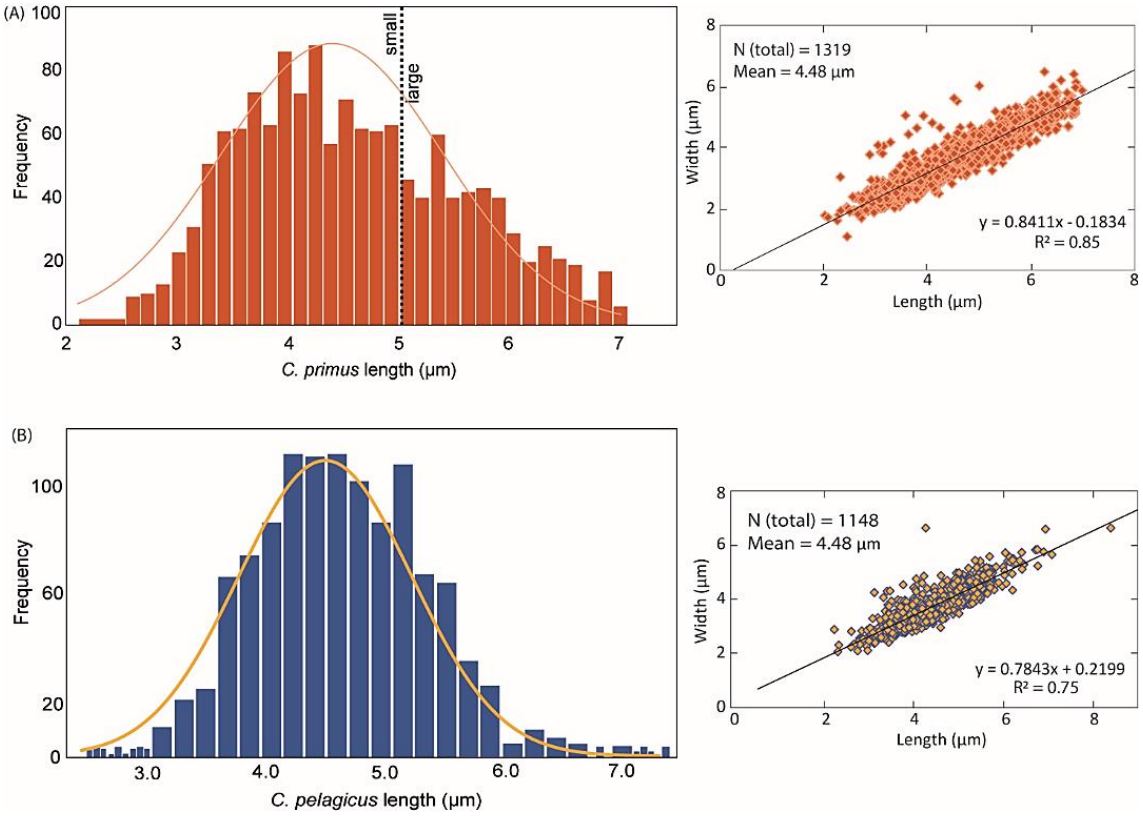

Figure 5. Frequency histogram distribution and scatter plots for morphometric analyses: coccolith width × length, mean size, and total of measures for *C. primus* (A) and *C. pelagicus* (B).

Median measures from box plot distribution show ranges from 3.44 to 5.10 µm to *C. primus* specimens. We identified three distinct intervals (Fig. 6A). Intervals 1 (108.74 to 107.82 m) and 2 (107.72 to 106.74 m) have similar median values (4.35 and 4.31 µm, respectively) with a slight increase, of ~0.7 µm, through interval 3 (106.54 to 106.15 m, median = 5.03 µm). (Fig.6B).

The distributions shown in *C. pelagicus* box plots do not show a clear trend, with the median values varying from 4.06 to 5.06 µm. We identified two intervals with a slight difference of ~0.60 µm (Fig. 6C), interval 1 (108.74 to 106.54 m) with median value of 4.38 µm and interval 2, the top of the section (106.35 to 106.15 m), having a median value of 4.98 µm (Fig. 6D).

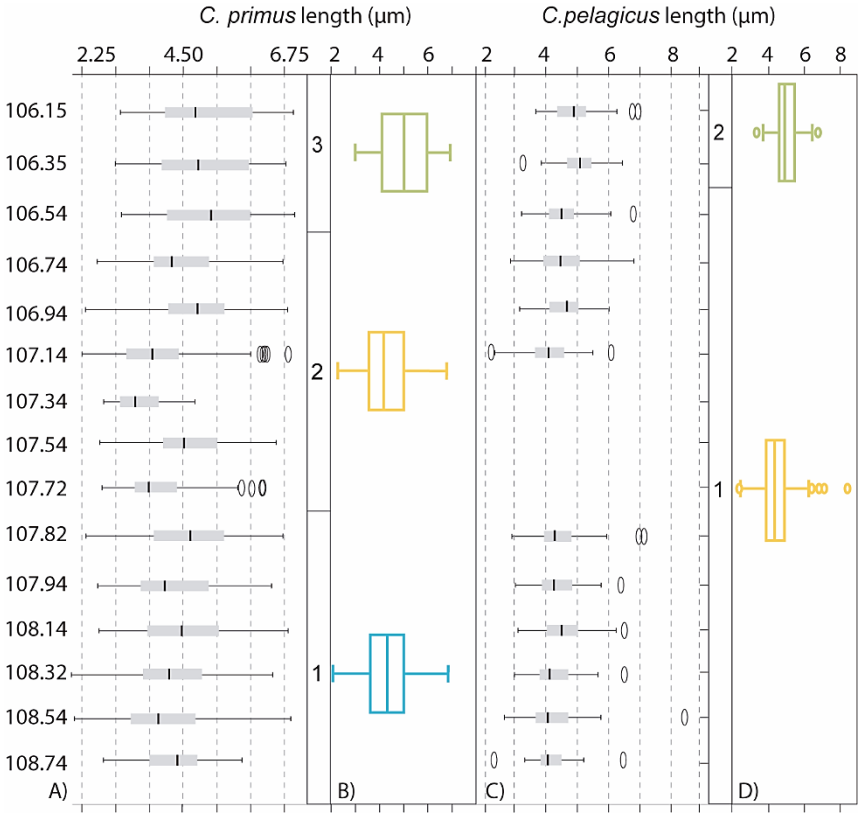

Figure 6. Size evolution of selected calcareous nannofossil species across the study interval. A, C) Box plots of *C. primus* (A) and *C. pelagicus* (C) with minimum and maximum measurements, the 25th and 75th percentiles, and median values; B, D) Box plots of relevant intervals for *C. primus* (B) and *C. pelagicus* (D). Intervals 1, 2 and 3 shown size pattern as described in the chapter 3.1.2.

3.3. X-Ray fluorescence analyses

The Fe/K ratio show three main trend intervals; one interval with stable and low values (from 112.37 m to 108.92 m), and two sharp increases (at 108.54 m and from 106.94 to 106.74 m).

The K/Ti ratio also presents similar trend, with one interval of stability (from 112.37 m to 108.92 m). However, we observe a slight decrease within this interval from 110.93 to 110.52 m. We further recorded two main sharp declines in K/Ti ratio in similar positions to increases in the Fe/K ratio (at 108.54 m and from 106.94 to 106.74 m).

There is a clear trend between terrigenous supply values (Terrigenous/Ca ratio) that increase alongside a decrease in biogenic production (Ca/Fe ratio): (i) the first interval occurs from 110.93 to 110.52 m; (ii) the second one occurs at 108.54 m; (iii) the last interval was recognized from 106.94 to 106.74 m. All XRF ratios are reported in Fig. 7

3.4. Calcium carbonate and total organic carbon content

Mean percentage in $CaCO_3$ content (Fig. 7) at our study site is 66 wt%, reaching the highest value 79 wt% at 106.35 m. Our record show three intervals with lower calcium carbonate contents: (i) from 112.37 to 110.52 m with an average of 58 wt%; (ii) an abrupt drop to the lowest values in the section (43.15 wt% at 108.54 m); and, (iii) the two samples with low values (106.94 and 106.74 m; mean value of 46.65 wt%). TOC percentages are low during the entire interval, and the mean value recorded is 0.12 % (ranging from 0.09 to 0.17 %). (Fig. 7)

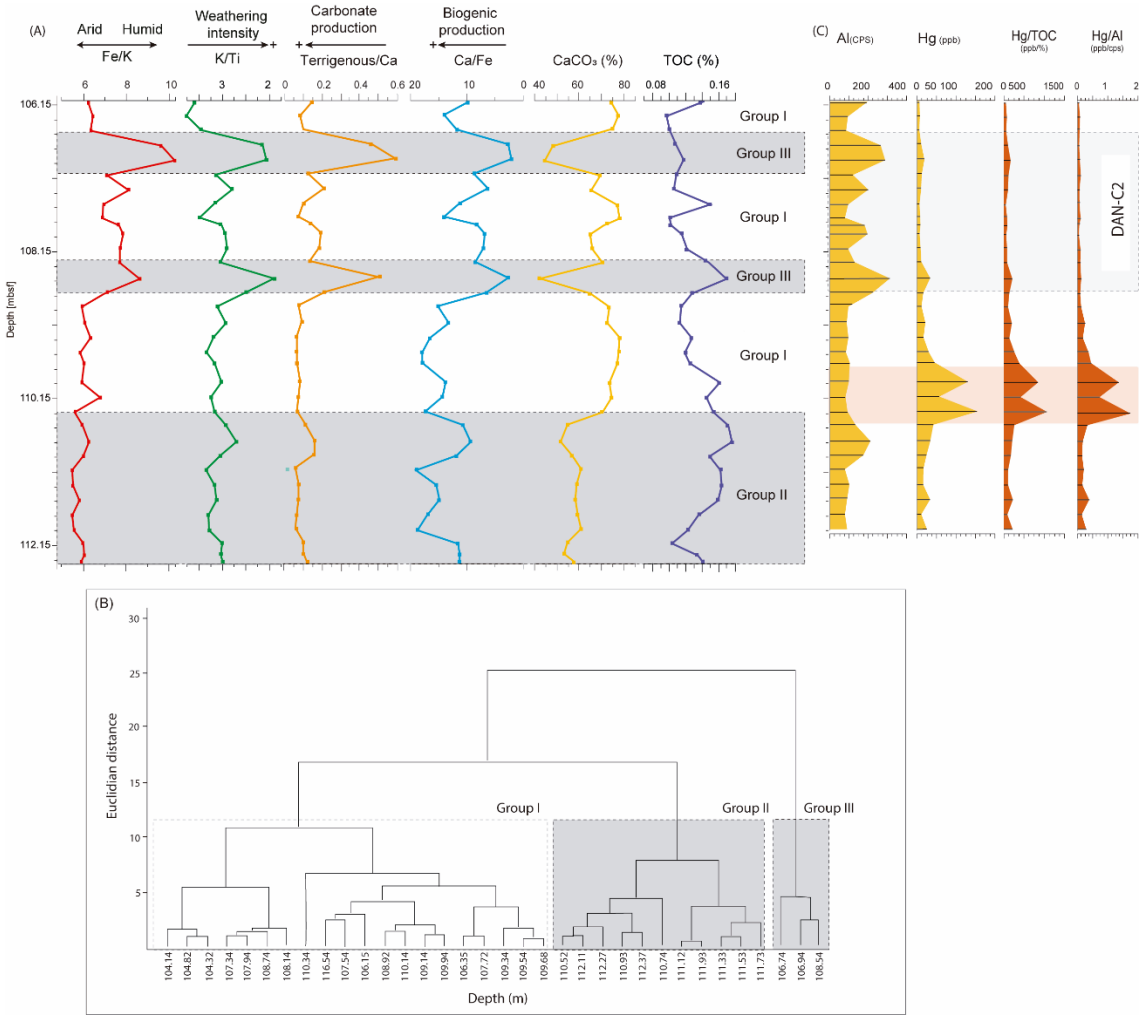

Fig. 7. A) Geochemical proxies applied at ODP site 1049C through XR-fluorescence, $CaCO_3$, and TOC content; B) Cluster groups defined in the section applying the coefficient of Euclidean distance and the UPGMA strategy (Unweighted Pair Group Method using Arithmetic Averages); C) Aluminium (Al), Mercury (Hg) and normalized concentration ($Hg/TOC_{ppb/\%}$ and $Hg/Al_{ppb/cps}$).

3.5. Multivariate statistical analyses

We define three different groups of sediments based on their geochemical affinities by applying cluster analysis (Fig. 7).

(i) Group I sediments (110.34 to 108.74; 108.32 to 107.14; and 106.54 to 106.15 m) is defined here by the high calcium carbonate content. This group also presents low

TOC values, increase in Ca/Fe and K/Ti ratio, alongside a decline in terrigenous/Ca and Fe/K ratios.

(ii) Group II sediments (112.37 to 110.52 m) are featured by low values of Fe/K, K/Ti, and Terrigenous/Ca ratio, alongside a decrease in carbonate production (through $CaCO_3$ and Ca/Fe ratio), and increase in TOC content.

(iii) Group III sediments (108.54 m, 106.94 and 106.74 m) is marked by abrupt changes in geochemical signals. The main feature is the increase Fe/K, Terrigenous/Ca and TOC content, there is also a decline in K/Ti ratio and carbonate/biogenic content ($CaCO_3$ and Ca/Fe ratio).

3.4. Mercury concentrations

The Hg concentrations (Fig. 7) for the analysed section (from 111.93 to 106.15 m) are low (average of 14.08 ppb). However, there is a clear interval with elevated concentrations (from 110.34 to 109.94 m). These samples have a Hg average of 129.47 ppb and highest values reaching 154.73 ppb (110.34 m). This sharp increase in the concentrations is also observed after normalizing to $Hg/TOC_{(ppb/\%)}$ and $Hg/Al_{(ppb/cps)}$ ($839.4_{(ppb/\%)}$ and $1.35_{(ppb/cps)}$, respectively).

4. Discussion

4.1. Calcareous nannofossils biohorizons at Blake Nose region

The difficulty in correlating incoming Paleogene calcareous nannofossils species in different sections is well recorded in Western Tethys studies (see Thibault et al., 2018). This variability in different basins can be attributed to the calcareous nannofossils' heterogeneous recovery after mass extinction (Jiang et al., 2010; Schueth et al., 2015). Northern Hemisphere was the most affected with calcareous nannofossil extinctions and the recovery was delayed in ~300 kyr (Jiang et al., 2010). Further, the lack of competition enables the earliest first appearance of a few incoming taxa (e.g., C.

pelagicus and *C. primus*) in North Hemisphere, and then in other basins (Mai et al., 2003; Schueth et al., 2015). Here we compare calcareous nannofossils biohorizons recorded in ODP Site 1049C, Blake Nose region (Fig. 2), with other sections deposited in the same interval (Bown, 2005; Bernaola and Monechi, 2007; Agnini et al., 2014; Thibault et al., 2018).

Although we do not record FO of *C. pelagicus* and *C. primus*, we recognized these species at the base of the section with similar trends (from 65.98 Ma). These species show rare to very low abundances (0 to 2 %) during the first 3.83 m of the section (up to ~0.21 Ma after K/Pg) that can be correlated with the NP1 Zone of Martini et al. (1971). Regarding *C. primus*, similar finds were recorded in Shatsky Rise (Bown, 2005), central Tunisia and southwest of France (Thibault et al., 2018). These authors recognized FO of *C. primus* and *C. primus* small (< 5 µm) at the top of NP1 Zone. Therefore, assuming FO of *C. primus* at 65.98 Ma (Thibault et al., 2018), it would be consistent with our age-depth model (Fig. 2).

However, strong diachroneity is observed in the FO of *C. pelagicus*. This species is only found at NP2 Zone at the Western Tethys section (Thibault et al., 2018) and in the biohorizon derived from age model (Agnini et al., 2014). Analysing Walvis Ridge records in the same interval as this study, we also noticed rare abundances of *C. pelagicus* (< 4 specimens). On the other hand, small morphotypes of *C. pelagicus* are found in abundance earliest (NP1 Zone) from Shatsky Rise (Bown, 2005). Considering this diachronous, the FO of *C. pelagicus* of 65.782 Ma derived from Agnini et al. (2014) does not appear to be according with our age model that suggests its FO occurs earlier in the Blake Nose section.

Cruciplacolithus intermedius appear in our section after *C. pelagicus*, which is according with CNP biohorizons (Agnini et al., 2014). However, its first occurrence age

of 65.709 Ma (Barnet et al., 2018) did not fall within our age model, suggesting the earliest occurrence at Blake Nose. First occurrence of *P. dimorphosus* group also have difference through sections. In this study, we recorded FO of *P. dimorphosus* group after *C. pelagicus*, as reported for Bidart Section from southwest of France (Thibault et al., 2018). However, FO of *P. dimorphosus* group of 65.902 Ma (Barnet et al., 2018) did not appear to be according to our age model, suggesting a late occurrence in our section (Fig. 2). This different record could be either due to difficulty of recognizing this specie in microscopy reading (< 2 μm) or diachronous in different basins, as evidenced by other species in this interval.

4.2. The role of volcanism during the DAN-C2 event

Abrupt increase in early Danian atmospheric pCO_2 levels are often ascribed to Deccan Traps CO_2 outgassing (Coccioni et al., 2010; Krahl et al., 2020). However, reconciling the geochemical features of the DAN-C2 event with volcanic activity has been questioned regarding timing and magnitude of Deccan eruption (Schoene et al., 2019; Sprain et al., 2019) and the orbital pacing signature of the event (Quillévéré et al., 2008; Arreguín-Rodríguez et al., 2021; Gilabert et al., 2021). Moreover, since the Ambenali Formation, India (Schoene et al., 2019, 2021), precedes the onset of DAN-C2 negative excursion, orbital forcing is thought to reasonably explain the amplification of atmospheric pCO_2 levels (Gilabert et al., 2021).

Our records show major increases in both $Hg/TOC_{(ppb/\%)}$ and $Hg/Al_{(ppb/cps)}$ concentrations from 110.34 to 109.94 m depth. Volcanic activity is thought to be a major natural source of mercury (Hg) in the atmosphere/ocean system, and strongly long-distance transported from emission sources (Pyle and Mather, 2003; Martin et al., 2012; Bagnato et al., 2014; Coufalík et al., 2018). In continental eruptive volcanic plumes, Hg is mostly emitted as gaseous elemental mercury (Hg^0), which is transported

mainly by the action of wind with an atmospheric residence-time of 0.5–2 years (Lindqvist and Rodhe, 1985; Lindberg et al., 2007; Ariya et al., 2008). In modern marine environments, primary source of mercury input is atmospheric deposition (Mason et al., 2012). In addition, submarine hydrothermal events have a significant contribution with Hg-rich fluids expelled during basalt-seawater interactions (Scaife et al., 2017). Other sources of Hg input constitute smaller fluxes, such as riverine discharge (Mason et al., 2012). The pattern of water-marine distribution of Hg mostly depends on the direction and intensity of ocean currents transporting Hg from source to sink, as well as the flux size and any changes to the global oceanic Hg residence time (Scaife et al., 2017). In modern oceans, Hg has a short (< 1 kyr) residence time (Scaife et al., 2017), and the rates of mercury accumulation in marine sediments are mainly controlled by biological productivity and organic matter burial (Sanei et al., 2012; Grasby et al., 2013). By normalizing Hg against TOC and Al (Fig. 8), we demonstrate that organic matter, and/or clay content are not primary controls of Hg fluctuations. Based on our age-depth model, we dated the Hg-rich layer in our records at ~65.90 Ma, which is strongly consistent with age estimates from the Ambenali Formation maximum eruption rate (Schoene et al., 2019). Our data suggest the volcanic activities preceded in ~70 kyr the DAN-C2 first negative $\delta^{13}C$ excursion (Fig. 8).

Large volcanic eruptions were major drivers of greenhouse gas inputs to the atmosphere/oceans systems and biological crises in the geological past (e.g. Burgess, 2019), the majority of these gases are in the form of H_2O, CO_2, N_2, and CH_4, (Robock, 2000). However, volcanic ash also contains micronutrients concentrations that can enhance ocean biological productivity in regions with low chlorophyll production (Watson, 1997; Duggen et al., 2007; Browning et al., 2014).

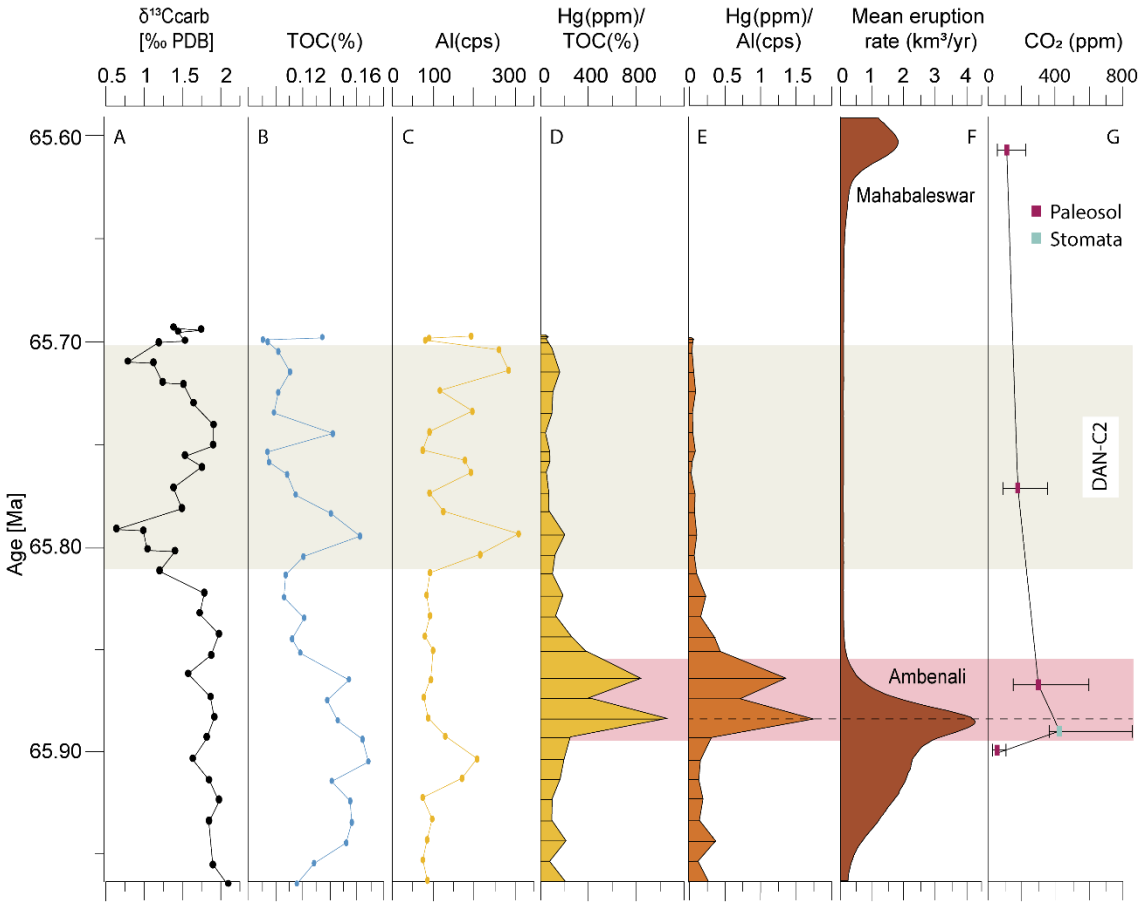

Figure 8. Correlation between the DAN-C2 event and volcanic activity records from Blake Nose and India. A) Bulk carbonate $\delta^{13}C$ (Quillévéré et al. (2008)); B) Total organic carbon (TOC) content; C) Aluminum measures; D-E) Volcanic activity evidence through $Hg_{(ppm)}$ normalized against $TOC_{(\%)}$ (D) and $Al_{(cps)}$ (E); F) Mean eruption rate in India (Schoene et al. (2019)); G) CO_2 estimates based on paleosol and stomata (Foster et al., 2017).

These interactions between ocean/atmosphere and the volcanic activities at Blake Nose region likely explain the continuous high biological productivity prior the DAN-C2. This is evidenced by the increase of $CaCO_3$ percentage from 110.34 to 108.92 m and biogenic production (Ca/Fe ratio) (Fig.7).

Furthermore, we noticed a continuously high abundances of *F. petalosa*, a small-size species (< 2 µm), mixotrophic taxon (Gibbs et al., 2020) with a fast growth rate. This species is highly abundant in shelf sediments and can be associated with high

productivity and less stratified waters (Gardin and Monechi, 1998; Coccioni et al., 2010). Moderate positive correlation (r = 0.469) between *F. petalosa* and $CaCO_3$ (Fig. 9) indicates that this species is favoured by increased $CaCO_3$ content through the section. Additionally, increased biogenic production prior to the DAN-C2 event could favour the better preservation signal observed in calcareous nannofossils assemblages (Fig. 5G-I).

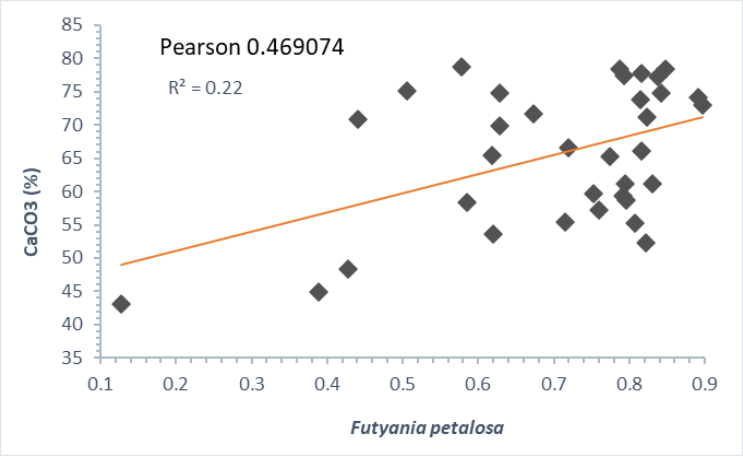

Fig. 9. Correlation between *Futyania petalosa* and Calcium carbonate data.

4.3. Disturbances in the carbon cycle across the DAN-C2 event

The magnitude of DAN-C2 at Blake Nose, i.e. the average between both negative CIEs in $\delta^{13}C$ (~1.2 ‰: Quillévéré et al., 2008), is either similar or, more often, comparatively larger than elsewhere: ~1.1 ‰ at the DSDP Site 527 (Quillévéré et al., 2008); ~0.6 ‰ at Zumaia, Spain (Gilabert et al., 2021); ~0.6 ‰ at Gubbio, Italy (Coccioni et al., 2010); ~0.5 ‰ at the DSDP Site 516F (Krahl et al., 2020); and ~0.7 ‰ at the ODP Site 1262 (Arreguín-Rodríguez et al., 2021). Comparison with classical, Paleocene hyperthermal events, such as the PETM (~4 ‰: Foster et al., 2018), shows that the DAN-C2 event also represents a major disturbance in the carbon biogeochemical cycle during the Paleogene.

The influence of carbon dioxide in calcareous nannofossil calcification rate is a matter of longstanding debates in proxy-based studies (Raffi and De Bernardi, 2008;

Raffi et al., 2009; Erba et al., 2010; O'Dea et al., 2014; Bottini and Faucher, 2020; Möller et al., 2020) and laboratory culture (Langer et al., 2006; Faucher et al., 2019). In general, the increase of CO_2 in the water column has a negative impact on ocean pH, reducing carbonate ion (CO_3^{2-}) and the carbonate saturation state ($\Omega < 1$), shoaling the carbonate compensation depth (CCD) and $CaCO_3$ dissolution, and hence affecting marine organism that precipitate $CaCO_3$ (e.g. Ridgwell and Zeebe, 2005; Cyronak et al., 2016). In addition, impacts on coccolith calcification have been reported during hyperthermal events (e.g., PETM), causing an increase of weak calcifiers and malformed species (Raffi and De Bernardi, 2008; Raffi et al., 2009) and decreasing size of dominant coccoliths usually at the event onset (O'Dea et al., 2014).

Analyses of coccolith size on both *C. pelagicus* and *C. primus* across ^{13}C-depleted intervals (CIEs) show the relationship between reducing coccolith size (*C. pelagicus*-0.6 and *C. primus*-0.72) and ^{12}C-rich water column (Fig. 10). This evidences the direct impact in carbonate ion available to precipitate $CaCO_3$ by calcareous nannoplankton organisms during CO_2 increases in water column. In fact, paleosol-based proxies show progressive drop in carbon dioxide levels across the DAN-C2 event, from similar-to-modern (~300-400 ppm) to pre-industrial levels (<180 ppm) (Foster et al., 2017) (Fig. 8), suggesting coeval CO_2 drawdown from atmosphere.

Calcium carbonate dissolution with CCD shoaling during DAN-C2 had been observed at Gubbio, Italy, Site DSDP 516F, Rio Grande Rise (Coccioni et al., 2010; Krahl et al., 2020), and Site ODP 1049C, Blake Nose (Quillévéré et al., 2008). However, considering that dissolution effects vary with depth, we observed that deeper basins (1500-3000 m paleodepth) in South Atlantic (ODP Site 1262) show $CaCO_3$ concentrations ranging between ~0 % (ODP Site 1262, Arreguín-Rodríguez et al., 2021) and 13 % (DSDP Site 516F, Krahl et al., 2020). In shallower basins (1000-1600 m

paleodepth) in North Atlantic (Gubbio, Coccioni et al., 2010; Zumaia, Gilabert et al., 2021), however, $CaCO_3$ concentrations during DAN-C2 reach ~43 % (Blake Nose, North Atlantic), 51 % (Zumaia, Spain), and even ~70 % (Gubbio, Italy). It is noteworthy that *C. pelagicus*, a dissolution-resistant taxon (Roth, 1994), is highly abundant during this dissolution interval at Blake Nose.

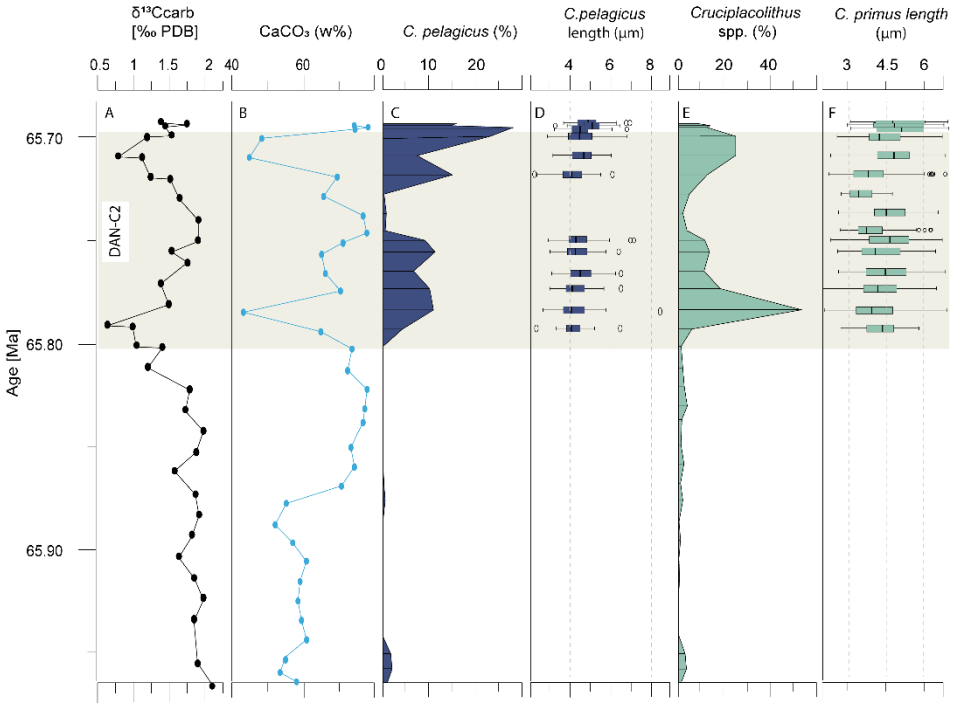

Figure 10. Carbon cycle dynamics across the DAN-C2 event at Blake Nose. A) Bulk carbonate $\delta^{13}C$ (Quillévéré et al. (2008)); B) Calcium carbonate content at Blake Nose; C-D) *Coccolithus pelagicus* relative abundance (C) and morphometric evolution (D); E-F) and *Cruciplacolithus primus* relative abundance (E) and morphometric evolution (F).

4.4. Multi-proxy evidence of terrigenous input during the DAN-C2 event

Biotic (calcareous nannofossil) and geochemical signals suggest that substantial increase in both fertility-indicative species and weathering-driven terrigenous supply mark the DAN-C2 event in our records at Blake Nose (from 108.54 m) (Fig. 11).

Calcareous nannofossil-based diversity (H) and equitability index (E) increase at the onset of DAN-C2 (Fig. 3). Similar pattern is also recorded at the Gubbio section,

Italy (Coccioni et al., 2010). However, calcareous nannofossil diversity at ODP Site 1049C is still considerably lower compared to Maastrichtian patterns (H > 2.4) (Linnert and Mutterlose, 2009). More evenly distributed calcareous nannofossil assemblage, followed by sharp increases in the abundance of *C. primus* and *C. pelagicus*, replaces the dominance of *F. petalosa*. Correlation analyses between *F. petalosa* with *C. pelagicus* and *C. primus* present strong negative values (r = 0.68, and r = -0.90, respectively) (Fig. 12), which strongly suggests that distribution pattern of *Coccolithus* species mirrors the total abundance of *F. petalosa*. These changes could be ascribed to either decreased productivity due to declining abundance of *F. petalosa*, dissolution effects (Fig. 5D-F), or closed-sum effect with *C. pelagicus* and *C. primus* abundances during this interval.

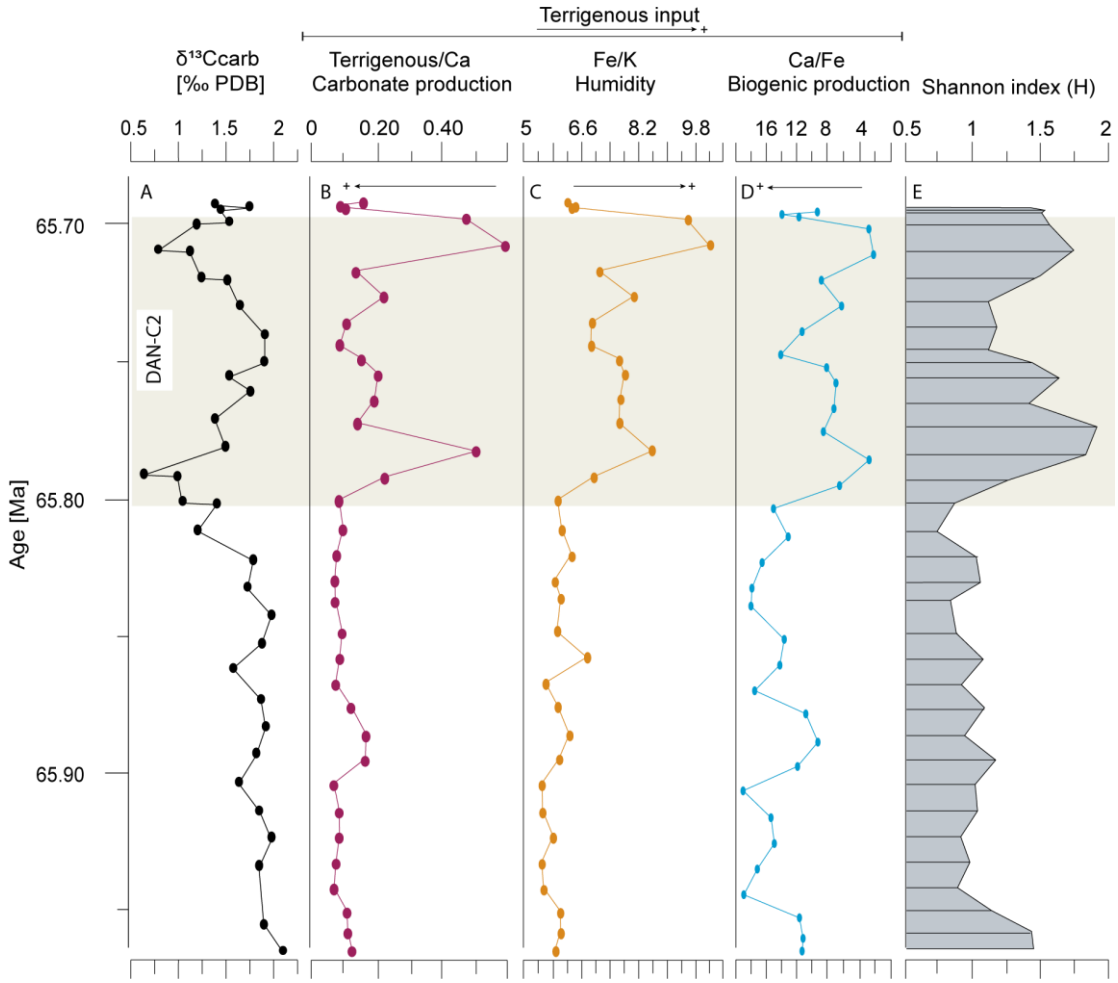

Figure 11. Selected indicators for terrigenous input. A) Bulk carbonate $\delta^{13}C$ (Quillévéré et al., 2008); B) Carbonate production based on Terrigenous/Ca ratio; C) Humid/arid climate conditions based on Fe/K ratio; D) Biogenic production based on Ca/Fe ratio; E) Shannon diversity Index (H).

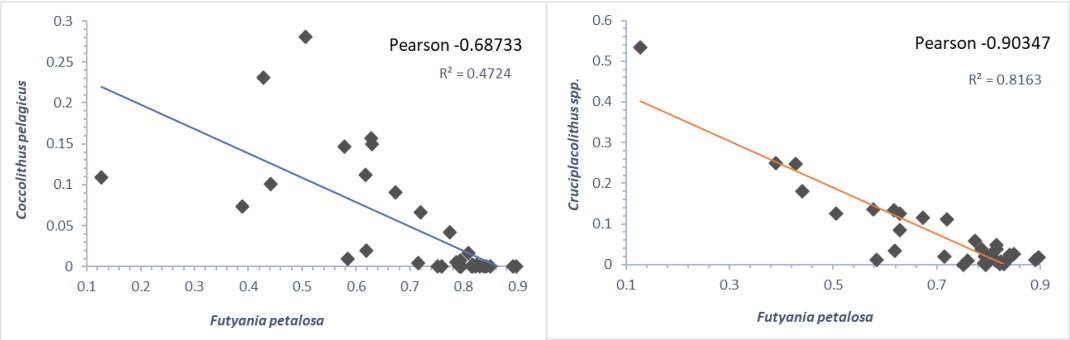

Figure 12. Correlations between *Futyania petalosa* and *Coccolithus pelagicus* and *Cruciplacolithus primus* abundances.

The co-occurrence of *C. pelagicus* and *C. primus* is evidenced by their strong correlation (r = 0.610) (Fig. 13), which indicates that both species have a similar ecological preference at the Blake Nose section. The first appearance of *C. primus*, in the geological record, is considered an indicator of a return to more stable environment conditions (Gardin and Monechi, 1998; Gardin, 2002) and oligotrophic waters (Jiang et al., 2010) after calcareous nannofossils mass extinction. However, at the Blake Nose section the abundance pattern of this species is proportional to *C. pelagicus* abundances within an interval of likely unstable conditions (DAN-C2). Thus, we suggested that enhanced nutrient supply in early Danian at Blake Nose region influence the relative abundance of *C. primus*. Other genera such as *Cervisiella* spp and *Braarudosphaera* spp. are present across the DAN-C2 major perturbation. Both genera are considered eutrophic indicators (Shimabukuro, 1994; Cunha and Shimabukuro, 1997; Kelly et al., 2003; Coccioni et al., 2010; D'Onofrio et al., 2016; Guerra et al., 2021), which

corroborate with enhanced nutrient supply during this interval. We concluded that this climate condition favoured eutrophic calcareous nannofossil species during the DAN-C2 event at Blake Nose.

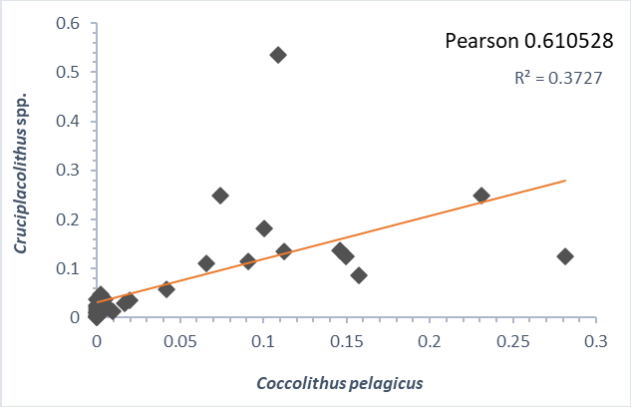

Figure 13. Correlation between *Cruciplacolithus primus* and *Coccolithus pelagicus* abundances.

High abundances of *C. pelagicus* occur alongside a decline in $\delta^{13}C$ measured in bulk samples (Quillévéré et al., 2008). This disagrees with previously recorded *C. pelagicus* blooms during an increase in $\delta^{13}C$ across the K/Pg boundary at sections from Egypt (Tantawy, 2003). *Coccolithus pelagicus* presents ecological preferences for eutrophic condition waters (Winter et al., 1994; Thierstein et al., 2004; D'Onofrio et al., 2016), and upwelling systems with enhanced nutrients and moderate turbulence (Cachão and Moita, 2000). Furthermore, the Blake Nose region was located in an upwelling system with abundant organic flux to the seafloor (Widmark and Speijer, 1997) during Maastrichtian. This condition persisted in the early Danian as demonstrated by benthic foraminifera studies (Alegret and Thomas, 2004). This interval is also marked by an increase in terrigenous supply as shown by sharp increases Terr/Ca ratios and reduction of biogenic production (Ca/Fe) (Fig.11). Thus, the enhanced

nutrient supply in the water column accompanied by a productive upwelling system during early Danian could favour the increase in *C. pelagicus* abundance in this interval.

4.5. Uncertainties in temperature estimates across the DAN-C2 event

Studies on calcareous nannofossil distribution suggest divergent SST preference for *C. pelagicus*, from warm (Eshet and Almogi-Labin, 1996; Tantawy, 2003; D'Onofrio et al., 2016) to cool surface waters (Rahman and Roth, 1990; Winter et al., 1994; Baumann et al., 2005). Despite being a major component of our calcareous nannofossil assemblage during the DAN-C2 event, we contend the high relative abundance (< 30 %) presented by *C. pelagicus* is mainly controlled by nutrient supply and eutrophic conditions, rather than changes in SST. This is consistent with both previous works on ecological preferences of *C. pelagicus* (Winter et al., 1994; Thierstein et al., 2004; D'Onofrio et al., 2016), and our multi-proxy records of substantial terrigenous input at Blake Nose (see item 4.4). Future studies should consider these effects prior to constrain SST estimates across the DAN-C2 event (Arreguín-Rodriguez et al. (2021).

In previous records, the DAN-C2 event is often characterized as a hyperthermal event (Quillévéré et al., 2008; Coccioni et al., 2010; Gilmour et al., 2013;), marked by a ~4°C transient warming in surface waters, as recorded by planktic foraminifera $\delta^{18}O$ data (Quillévéré et al., 2008). However, the lack of independent sea-surface and deep-ocean temperature estimates raises question on such estimates from planktic foraminifera (Quillévéré et al., 2008) due to different factors affecting the $\delta^{18}O$ isotopic signals (e.g., salinity, Katz et al., 2010) (Arreguín-Rodriguez et al., 2021). This has challenged the view of the DAN-C2 as a hyperthermal event (Arreguín-Rodríguez et al., 2021).

Here we correlate independent sea-surface temperature (SST) proxies: local $\delta^{18}O_{carb}$ [‰ PDB] (Quillévéré et al., 2008) and TEX_{86} from Brazos River (US Gulf Coast) and Miers Farm (US East Coast), and Bajada del Jagüel (eastern Argentina) (Hull et al., 2020). Despite poor time coverage for this interval, mean values show a slight decline (~ 1.5 ºC) in SST from 65.80 to 65.70 Ma, even at sites located closer to the study area (Fig. 14). This TEX_{86}-based cooling trend contradict previously thought warming trend (~ 4 °C) based on planktic foraminifera $\delta^{18}O_{carb}$ at Blake Nose (Quillévéré et al., 2008). Declining temperatures observed during the DAN-C2 event, however, are strongly consistent with gradual decrease in atmosphere carbon dioxide levels across the same interval (Foster et al., 2017) (as also discussed in chapter 4.3).

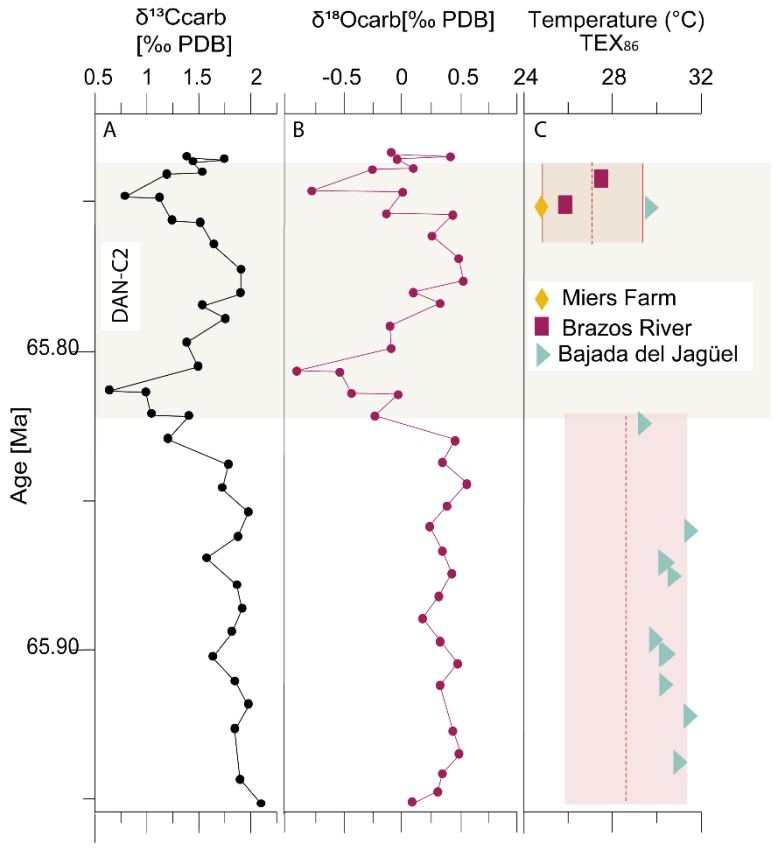

Figure 14. Sea-surface temperatures estimates during the DAN-C2 event. A-B) Bulk carbonate $\delta^{13}C$ (A) and $\delta^{18}O$ (B) (Quillévéré et al. (2008); C) TEX_{86} compilation from elsewhere (Hull et al. (2020) – Miers Farm (US East Coast), Brazos River (US Gulf Coast), and Bajada del Jagüel (eastern Argentina).

4.6. The DAN-C2 event and implications for the global climate system

To explain the delivery of large amounts of terrigenous-rich sediments to the Blake Nose region, we assessed two potential sources: direct supply from the North American eastern coast and the Gulf Coastal Plain via an invigorated Gulf Stream. Proxy-based studies of terrestrial organic matter in sediments show evidence of soil-derived biomarkers across the eastern and southern coast of the United States (Hull et al., 2020). Records of Branched and Isoprenoid Tetraether (BIT) index spanning 66.01 to 65.70 Ma from Brazos River (US Gulf Coast) and Miers Farm (US East Coast) are similar between 66.01 and 65.98 Ma. However, from 65.98 Ma and coeval with the DAN-C2 event, we notice the onset of a significant gradient between BIT indices from both areas. This is evidence of a differential increase in fluvial activity in the Brazos River area relative to Miers Farm (Fig. 15). Present-day Brazos River drainage basin flows into the Gulf of Mexico. This was likely similar in Paleocene times (Lee and Singh, 2020), when Florida was a submerged platform and an open pathway to the Blake Plateau for a proto-Gulf Stream (Pinet and Popenoe, 1985).

The onset of Gulf Stream circulation over the Blake Plateau is uncertain (Watkins and Self-Trail, 2005). Existing records suggest an easterly current flow through Suwannee Strait in southern Georgia and northern Florida, being this flow the responsible for excessive amount of water and clastic sediment into the western Blake Plateau basin from Late Cretaceous to Paleocene (Pinet and Popenoe, 1985). In addition, other studies have reported the influence of Gulf Stream in Late Cretaceous by changes in surface water temperatures, nutrient supply, and calcareous nannofossils assemblages (Linnert and Mutterlose, 2009; Watkins and Self-Trail, 2005). These Cenozoic records hypothesize that global fluctuations in sea level were the main drivers of the Gulf Stream displacement, from a northerly flow towards the Florida-Hatteras

Slope to a northeasterly flow towards the Blake Plateau (Pinet and Popenoe, 1985). However, recent model simulations show that CO_2 doubling also lead to a northerly shift of the Gulf Stream impacting in salinity and warming temperatures at Northwest Atlantic shelf (Saba et al., 2015).

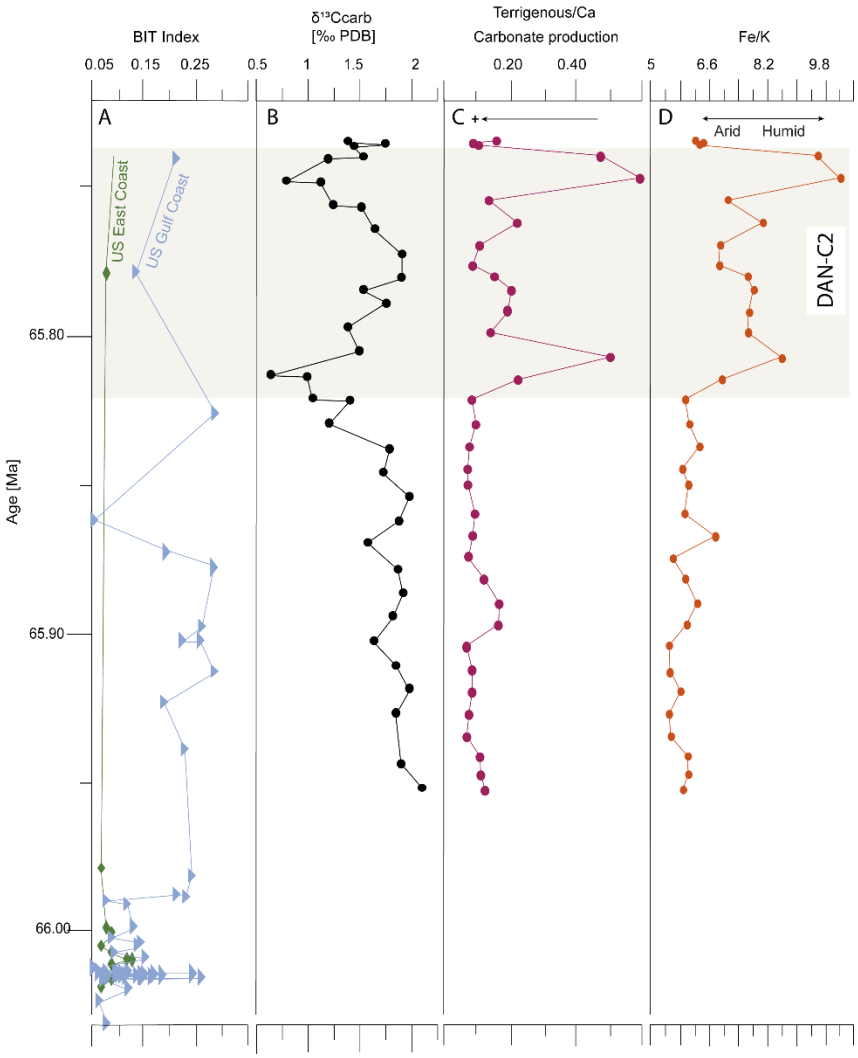

Figure 15. Correlation between fluvial activity in western North Atlantic and terrestrial input from the Blake Nose area. A) BIT Index from Brazos River (blue triangle) and Miers Farm (green diamond) (Hull et al., 2020); B) Bulk carbonate $\delta^{13}C$ (Quillévéré et al. (2008); C-D) Selected indicators of continental input (this study).

Eccentricity maximum cycles (most elliptical orbit shape) cause variations between perihelion and aphelion temperatures, and it also amplifies precession cycles causing an increase in CO_2 release (Ruddiman, 2014; Barnet et al., 2018, 2019). This

may have enhanced the effects of moderately high CO_2 climate state by triggering seasonal invigoration of hydrological cycle and shifts in the patterns of surface ocean currents. This agrees with previous studies, which have associated the unstable conditions during DAN-C2 with orbital control (Quilléveré et al., 2008; Coccioni et al., 2010), being the duration of the event synchronous with eccentricity maximum $Pc_{405}1$ (Barnet et al., 2019; Gilabert et al., 2021).

We contend that the dynamics of surface ocean currents is the best mechanism to explain the observed features associated with the DAN-C2 event, especially when orbital-scale seasonality amplifies the effects of similar-to-today pCO_2 levels. Local changes in paleocirculation combined with sediment remobilizations from the Gulf of Mexico would have enhanced CO_2 drawdown, influencing the strongest negative ^{13}C excursion (~1.3 ‰) in Blake Nose compared to other areas (Coccioni et al., 2010; Arreguín-Rodríguez et al., 2021; Gilabert et al., 2021; Krahl et al., 2020).

5. Conclusion

Our high-resolution multi-proxy records from the ODP Site 1049C, Blake Nose, North Atlantic, provide new geochemical and microfossil data from 65.98 to 65.70 Ma. These yield significant biotic response to paleoclimate changes through the DAN-C2 event, the earliest carbon isotope excursion in the Paleogene.

At Blake Nose, our microfossil and XRF records show high productivity and arid environment pior to the DAN-C2 event. Here and for the first time we also provide the first records of Hg content for the interval. Increased Hg content at 65.90 Ma closely correlates with Ambenali formation (Deccan Traps), India, and previous carbon dioxide estimates. This likely impacts the increase of calcium carbonate content and biogenic production, leading to an improvement in calcareous nannofossils preservation.

The DAN-C2 event marks major changes in coccolith assemblages, such as high diversity, and abundant eutrophic and fertility-indicative species. Geochemical evidence shows increased weathering and terrigenous supply. We also provide new evidence demonstrating that reducing size of calcareous nannofossils (*C. pelagicus* and *C. primus*) across DAN-C2 event is linked to an interval of intense dissolution and pCO_2 sequestration.

Moreover, we present uncertainties in temperature estimates for DAN-C2 based on independent organic proxy data from compiled studies. These record a ~1.5 ˚C cooling trend across interval, which is associated with coeval pCO_2 drawdown from atmosphere.

Finally, we suggest that the dynamics of surface ocean currents are an important mechanism to explain the strongest $\delta^{13}C$ negative excursion observed in Blake Nose. Eccentricity maximum cycle likely amplifies the effects of similar-to-today pCO_2 levels, leading to local changes in paleo circulation combined with sediments remobilizations from Gulf of Mexico, and enhance pCO_2 drawdown to deep ocean sediments.

Acknowledgements

This study used samples from the International Ocean Drilling Program (IODP). The authors are grateful to MSc Edna J. F. Tungo, Dr Jorge Villegas-Martin for the interesting discussion about this interval. We thank Jordana S. Xavier and Lucas Oliveira from Itt Oceaneon for their laboratory skills with Hg concentration measures and SEM analyses. We also thank Professor Dr Nicolas Thibault and Dr Silvia Gardin for sharing personal experiences from end-Cretaceous calcareous nannoplankton assemblages, and Professor Dr Blair Schoene for sharing his data on the Deccan Trap

eruption rate. Special thanks to Professor Dr Léo Hartmann and Prof. Dr Francisco M. W. Tognoli for suggestions on the structure of this manuscript.

II. SÍNTESE INTEGRADORA

Este trabalho proporcionou uma melhor caracterização paleoecológica e geoquímica da região de Blake Nose (*Site* 1049C) durante a primeira excursão negativa de $\delta^{13}C$ do início do Daniano (DAN-C2). Com a análise de distribuição das espécies de nanofósseis calcários foi possível definir novas evidências de diacronismos relacionados ao surgimento de novas espécies após a extinção em massa do K/Pg. Além disso, foi possível correlacionar o padrão de distribuição das espécies mais abundantes com *proxies* paleoceanográficos e paleoclimáticos. Isto permitiu definir intervalos de alta e baixa produtividade, intervalos de maior aridez, intervalos de aumento de intemperismo e condições eutróficas e intervalos de atividade vulcânica. Todos estes intervalos apresentam uma resposta biótica, seja na forma de abundância ou no padrão morfológico das espécies de nanofósseis.

Para o evento DAN-C2, foi possível estabelecer um padrão na distribuição de nanofósseis calcários, evidenciado pelo aumento na diversidade e enriquecimento de espécies indicativas de alta fertilidade com preferência paleoecológica por ambientes ricos em nutrientes. Correlacionamos as espécies *Coccolithus pelagicus* e *Cruciplacolithus primus* (espécies mais abundantes durante o evento DAN-C2). Ambas as espécies apresentam preferências paleoecológicas similares nesse intervalo e podem ser usadas como indicadores de alta fertilidade. Também apresentamos nesse intervalo uma análise morfológica com base nessas duas espécies, indicando uma redução no tamanho dos espécimes durante as fases de instabilidade ambiental do DAN-C2. Essa redução de tamanho ocorre concomitante com o aumento nos níveis de CO_2 registrados em sedimentos marinhos.

Por fim, dados de mercúrio apresentados de forma pioneira nesse intervalo evidenciam atividades vulcânicas e impactos positivos na preservação de nanofósseis calcários da região aproximadamente 70 mil anos antes do evento DAN-C2. Esse dado é coerente com o aumento de *p*CO2 atmosférico no mesmo período. Com esse resultado evidenciamos que não há correlação direta entre a atividade vulcânica e o intervalo de excursão negativa de $\delta^{13}C$, debatido em estudos anteriores. Ademais, resultados obtidos na região de Blake Nose evidenciam forte influência de correntes oceânicas superficiais durante a deposição dos sedimentos do DAN-C2. Os dados apresentados por este manuscrito irão impactar diretamente no entendimento do evento DAN-C2 e da dinâmica do sistema climático terrestre em períodos de abruptos distúrbios no ciclo do carbono, a exemplo de cenários climáticos prospectivos.

References

Agnini, C., Fornaciari, E., Raffi, I., Catanzariti, R., Pälike, H., Backman, J., Rio, D., 2014. Biozonation and biochronology of Paleogene calcareous nannofossils from low and middle latitudes. Newsletters Stratigr. 47, 131–181. https://doi.org/10.1127/0078-0421/2014/0042

Alegret, L., Thomas, E., 2004. Benthic foraminifera and environmental turnover across the Cretaceous/Paleogene boundary at Blake Nose (ODP Hole 1049C, Northwestern Atlantic). Palaeogeogr. Palaeoclimatol. Palaeoecol. 208, 59–83. https://doi.org/10.1016/j.palaeo.2004.02.028

Alvarez, S.A., Gibbs, S.J., Bown, P.R., Kim, H., Sheward, R.M., Ridgwell, A., 2019. Diversity decoupled from ecosystem function and resilience during mass extinction recovery. Nature 574, 242–245. https://doi.org/10.1038/s41586-019-1590-8

Ariya, P.A., Skov, H., Grage, M.M.L., Goodsite, M.E., 2008. Gaseous Elemental Mercury in the Ambient Atmosphere: Review of the Application of Theoretical Calculations and Experimental Studies for Determination of Reaction Coefficients and Mechanisms with

Halogens and Other Reactants. Adv. Quantum Chem. 55, 43–55. https://doi.org/10.1016/S0065-3276(07)00204-3

Arreguín-Rodríguez, G.J., Barnet, J.S.K., Leng, M.J., Littler, K., Kroon, D., Schmidt, D.N., Thomas, E., Alegret, L., 2021. Benthic foraminiferal turnover across the Dan-C2 event in the eastern South Atlantic Ocean (ODP Site 1262). Palaeogeogr. Palaeoclimatol. Palaeoecol. 572, 110410. https://doi.org/10.1016/j.palaeo.2021.110410

Bagnato, E., Barra, M., Cardellini, C., Chiodini, G., Parello, F., Sprovieri, M., 2014. First combined flux chamber survey of mercury and CO2 emissions from soil diffuse degassing at Solfatara of Pozzuoli crater, Campi Flegrei (Italy): Mapping and quantification of gas release. J. Volcanol. Geotherm. Res. 289, 26–40. https://doi.org/10.1016/J.JVOLGEORES.2014.10.017

Barnet, J.S.K., Littler, K., Kroon, D., Leng, M.J., Westerhold, T., Röhl, U., Zachos, J.C., 2018. A new high-resolution chronology for the late Maastrichtian warming event: Establishing robust temporal links with the onset of Deccan volcanism. Geology 46, 147–150. https://doi.org/10.1130/G39771.1

Barnet, J.S.K., Littler, K., Westerhold, T., Kroon, D., Leng, M.J., Bailey, I., Röhl, U., Zachos, J.C., 2019. A High-Fidelity Benthic Stable Isotope Record of Late Cretaceous–Early Eocene Climate Change and Carbon-Cycling. Paleoceanogr. Paleoclimatology 34, 672–691. https://doi.org/10.1029/2019PA003556

Bernaola, G., Monechi, S., 2007. Calcareous nannofossil extinction and survivorship across the Cretaceous-Paleogene boundary at Walvis Ridge (ODP Hole 1262C, South Atlantic Ocean). Palaeogeogr. Palaeoclimatol. Palaeoecol. 255, 132–156. https://doi.org/10.1016/j.palaeo.2007.02.045

Bottini, C., Faucher, G., 2020. Biscutum constans coccolith size patterns across the mid Cretaceous in the western Tethys: Paleoecological implications. Palaeogeogr. Palaeoclimatol. Palaeoecol. 555, 109852. https://doi.org/10.1016/j.palaeo.2020.109852

Bown, P., 2005. Selective calcareous nannoplankton survivorship at the Cretaceous-Tertiary boundary. Geology 33, 653–656. https://doi.org/10.1130/G21566.1

Bown, P.R., Young, J.R., 1998. Techniques, in: Calcareous Nannofossil Biostratigraphy. Kluwer Academi, Dordrecht, p. 265.

Browning, T.J., Bouman, H.A., Henderson, G.M., Mather, T.A., Pyle, D.M., Schlosser, C., Woodward, E.M.S., Moore, C.M., 2014. Strong responses of Southern Ocean phytoplankton communities to volcanic ash. Geophys. Res. Lett. 41, 2851–2857. https://doi.org/10.1002/2014GL059364

Burgess, S., 2019. Deciphering mass extinction triggers. Science (80-.). 363, 815–816. https://doi.org/10.1126/science.aaw0473

Cachão, M., Moita, M.T., 2000. Coccolithus pelagicus, a productivity proxy related to moderate fronts off Western Iberia. Mar. Micropaleontol. 39, 131–155. https://doi.org/10.1016/S0377-8398(00)00018-9

Coccioni, R., Frontalini, F., Bancalà, G., Fornaciari, E., Jovane, L., Sprovieri, M., 2010. The Dan-C2 hyperthermal event at Gubbio (Italy): Global implications, environmental effects, and cause(s). Earth Planet. Sci. Lett. 297, 298–305. https://doi.org/10.1016/j.epsl.2010.06.031

Coufalík, P., Krmíček, L., Zvěřina, O., Meszarosová, N., Hladil, J., Komárek, J., 2018. Model of Mercury Flux Associated with Volcanic Activity. Bull. Environ. Contam. Toxicol. 2018 1015 101, 549–553. https://doi.org/10.1007/S00128-018-2430-5

Courtillot, V., Féraud, G., Maluski, H., Vandamme, D., Moreau, M.G., Besse, J., 1988. Deccan flood basalts and the Cretaceous/Tertiary boundary. Nature 333, 843–846. https://doi.org/10.1038/333843a0

Cunha, A.S., Shimabukuro, S., 1997. Braarudosphaera blooms and anomalous enrichments of Nannoconus: evidence from the Turonian south Atlantic, Santos basin, Brazil. J. Nannoplankt. Res. 19, 51–55.

Cyronak, T., Schulz, K.G., Jokiel, P.L., 2016. The Omega myth: what really drives lower calcification rates in an acidifying ocean. ICES J. Mar. Sci. 73, 558–562. https://doi.org/10.1093/icesjms/fsv075

D'Hondt, S., 2005. Consequences of the cretaceous/paleogene mass extinction for marine

ecosystems. Annu. Rev. Ecol. Evol. Syst. 36, 295–317. https://doi.org/10.1146/annurev.ecolsys.35.021103.105715

D'Hondt, S., 1998. Organic Carbon Fluxes and Ecological Recovery from the Cretaceous-Tertiary Mass Extinction. Science (80-.). 282, 276–279. https://doi.org/10.1126/science.282.5387.276

D'Onofrio, R., Luciani, V., Fornaciari, E., Giusberti, L., Boscolo Galazzo, F., Dallanave, E., Westerhold, T., Sprovieri, M., Telch, S., 2016. Environmental perturbations at the early Eocene ETM2, H2, and I1 events as inferred by Tethyan calcareous plankton (Terche section, northeastern Italy). Paleoceanography 31, 1225–1247. https://doi.org/10.1002/2016PA002940

Dinarès-Turell, J., Westerhold, T., Pujalte, V., Röhl, U., Kroon, D., 2014. Astronomical calibration of the Danian stage (Early Paleocene) revisited: Settling chronologies of sedimentary records across the Atlantic and Pacific Oceans. Earth Planet. Sci. Lett. 405, 119–131. https://doi.org/10.1016/j.epsl.2014.08.027

Duggen, S., Croot, P., Schacht, U., Hoffmann, L., 2007. Subduction zone volcanic ash can fertilize the surface ocean and stimulate phytoplankton growth: Evidence from biogeochemical experiments and satellite data. Geophys. Res. Lett. 34, L01612. https://doi.org/10.1029/2006GL027522

Erba, E., Bottini, C., Weissert, H.J., Keller, C.E., 2010. Calcareous nannoplankton response to surface-water acidification around Oceanic Anoxic Event 1a. Science (80-.). 329, 428–432.

Fabry, V.J., 2008. Marine Calcifiers in a High-CO 2 Ocean. Science (80-.). 320, 1020–1022. https://doi.org/10.1126/science.1157130

Faucher, G., Riebesell, U., Bach, L.T., 2019. Can morphological features of coccolithophores serve as a reliable proxy to reconstruct environmental conditions of the past? Clim. Past Discuss. 1–21. https://doi.org/10.5194/cp-2019-84

Font, E., Adatte, T., Sial, A.N., de Lacerda, L.D., Keller, G., Punekar, J., 2016. Mercury anomaly, deccan volcanism, and the end-cretaceous mass extinction. Geology 44, 171–

174. https://doi.org/10.1130/G37451.1

Foster, G.L., Hull, P., Lunt, D.J., Zachos, J.C., 2018. Placing our current “hyperthermal” in the context of rapid climate change in our geological past. Philos. Trans. R. Soc. A Math. Phys. Eng. Sci. 376. https://doi.org/10.1098/rsta.2017.0086

Frank, T.D., Arthur, M.A., 1999. Tectonic forcings of Maastrichtian ocean-climate evolution. Paleoceanography 14, 103–117. https://doi.org/10.1029/1998PA900017

Gardin, S., 2002. Late Maastrichtian to early Danian calcareous nannofossils at Elles (Northwest Tunisia). A tale of one million years across the K-T boundary. Palaeogeogr. Palaeoclimatol. Palaeoecol. 178, 211–231. https://doi.org/10.1016/S0031-0182(01)00397-2

Gardin, S., Monechi, S., 1998. Palaeoecological change in middle to low latitude calcareous nannoplankton at the Cretaceous/Tertiary boundary. Bull. la Société géologique Fr. 169, 709–723.

Gibbs, S.J., Bown, P.R., Ward, B.A., Alvarez, S.A., Kim, H., Archontikis, O.A., Sauterey, B., Poulton, A.J., Wilson, J., Ridgwell, A., 2020. Algal plankton turn to hunting to survive and recover from end-Cretaceous impact darkness. Sci. Adv. 6, eabc9123. https://doi.org/10.1126/sciadv.abc9123

Gilabert, V., Batenburg, S.J., Arenillas, I., Arz, J.A., 2021. Contribution of orbital forcing and Deccan volcanism to global climatic and biotic changes across the Cretaceous-Paleogene boundary at Zumaia, Spain. Geology XX, 1–5. https://doi.org/10.1130/g49214.1

Gilmour, I., Gilmour, M., Jolley, D., Kelley, S., Kemp, D., Daly, R., Watson, J., 2013. A high-resolution nonmarine record of an early Danian hyperthermal event, Boltysh crater, Ukraine. Geology 41, 783–786. https://doi.org/10.1130/G34292.1

Grasby, S.E., Sanei, H., Beauchamp, B., Chen, Z., 2013. Mercury deposition through the Permo–Triassic Biotic Crisis. Chem. Geol. 351, 209–216. https://doi.org/10.1016/J.CHEMGEO.2013.05.022

Guerra, R.M., Concheyro, A., Kochhann, K.G.D., Bom, M.H.H., Ceolin, D., Musso, T., Savian, J.F., Fauth, G., 2021. Calcareous microfossils and paleoenvironmental changes across the

Cretaceous-Paleogene (K-Pg) boundary at the Cerro Azul Section , Neuquén. Palaeogeogr. Palaeoclimatol. Palaeoecol. 567, 110217. https://doi.org/10.1016/j.palaeo.2021.110217

Hammer, O., Harper, D.A.T., Ryan, P.D., 2001. PAST : Paleontological Statistics Software Package for Education and Data Analysis PAST : Paleontological Statistics Software Package for Education and data analysis Even a cursory glance at the recent paleontological literature should convince anyone tha. Palaeontol. Electron. 4, 1–9.

Holbourn, A., Kuhnt, W., El Albani, A., Pletsch, T., Luderer, F., Wagner, T., 1999. Upper Cretaceous palaeoenvironments and benthonic foraminiferal assemblages of potential source rocks from the western African margin, Central Atlantic. Geol. Soc. Spec. Publ. 153, 195–222. https://doi.org/10.1144/GSL.SP.1999.153.01.13

Hughes, M., Swetnam, T., Diaz, H., 2015. Micro-XRF Studies of Sediment Cores, Developments in Paleoenvironmental Research. Springer Netherlands, Dordrecht. https://doi.org/10.1007/978-94-017-9849-5

Hull, P.M., Bornemann, A., Penman, D.E., Henehan, M.J., Norris, R.D., Wilson, P.A., Blum, P., Alegret, L., Batenburg, S.J., Bown, P.R., Bralower, T.J., Cournede, C., Deutsch, A., Donner, B., Friedrich, O., Jehle, S., Kim, H., Kroon, D., Lippert, P.C., Loroch, D., Moebius, I., Moriya, K., Peppe, D.J., Ravizza, G.E., Röhl, U., Schueth, J.D., Sepúlveda, J., Sexton, P.F., Sibert, E.C., Śliwińska, K.K., Summons, R.E., Thomas, E., Westerhold, T., Whiteside, J.H., Yamaguchi, T., Zachos, J.C., 2020. On impact and volcanism across the Cretaceous-Paleogene boundary. Science (80-.). 367, 266–272. https://doi.org/10.1126/science.aay5055

Hull, P.M., Norris, R.D., 2011. Diverse patterns of ocean export productivity change across the Cretaceous-Paleogene boundary: New insights from biogenic barium. Paleoceanography 26, 1–10. https://doi.org/10.1029/2010PA002082

Jiang, S., Bralower, T.J., Patzkowsky, M.E., Kump, L.R., Schueth, J.D., 2010. Geographic controls on nannoplankton extinction across the Cretaceous/Palaeogene boundary. Nat. Geosci. 3, 280–285. https://doi.org/10.1038/ngeo775

Katz, M.E., Cramer, B.S., Franzese, A., Hönisch, B., Miller, K.G., Rosenthal, Y., Wright, J.D., 2010. Traditional and emerging geochemical proxies in foraminifera. J. Foraminifer. Res. 40, 165–192. https://doi.org/10.2113/gsjfr.40.2.165

Keller, G., Mateo, P., Monkenbusch, J., Thibault, N., Punekar, J., Spangenberg, J.E., Abramovich, S., Ashckenazi-Polivoda, S., Schoene, B., Eddy, M.P., Samperton, K.M., Khadri, S.F.R., Adatte, T., 2020. Mercury linked to Deccan Traps volcanism, climate change and the end-Cretaceous mass extinction. Glob. Planet. Change 194, 103312. https://doi.org/10.1016/j.gloplacha.2020.103312

Kelly, D.C., Norris, R.D., Zachos, J.C., 2003. Deciphering the paleoceanographic significance of Early Oligocene Braarudosphaera chalks in the South Atlantic. Mar. Micropaleontol. 49, 49–63. https://doi.org/10.1016/S0377-8398(03)00027-6

Krahl, G., Bom, M.H.H., Kochhann, K.G.D., Souza, L. V., Savian, J.F., Fauth, G., 2020. Environmental changes occurred during the Early Danian at the Rio Grande Rise, South Atlantic Ocean. Glob. Planet. Change 191. https://doi.org/10.1016/j.gloplacha.2020.103197

Langer, G., Geisen, M., Baumann, K.H., Kläs, J., Riebesell, U., Thoms, S., Young, J.R., 2006. Species-specific responses of calcifying algae to changing seawater carbonate chemistry. Geochemistry, Geophys. Geosystems 7. https://doi.org/10.1029/2005GC001227

Lee, K., Singh, V.P., 2020. Analysis of uncertainty and non-stationarity in probable maximum precipitation in Brazos River basin. J. Hydrol. 590, 125526. https://doi.org/10.1016/j.jhydrol.2020.125526

Lindberg, S., Bullock, R., Ebinghaus, R., Engstrom, D., Feng, X., Fitzgerald, W., Pirrone, N., Prestbo, E., Seigneur, C., 2007. A synthesis of progress and uncertainties in attributing the sources of mercury in deposition, in: Ambio. pp. 19–32. https://doi.org/10.1579/0044-7447(2007)36[19:ASOPAU]2.0.CO;2

Lindqvist, O., Henning, R., 1985. Atmospheric mercury—a review. Tellus B 37 B, 136–159. https://doi.org/10.1111/j.1600-0889.1985.tb00062.x

Linnert, C., Mutterlose, J., 2009. Evidence of increasing surface water oligotrophy during the

Campanian-Maastrichtian boundary interval: Calcareous nannofossils from DSDP Hole 390A (Blake Nose). Mar. Micropaleontol. 73, 26–36. https://doi.org/10.1016/j.marmicro.2009.06.006

Mai, H., Speijer, R.P., Schulte, P., 2003. Calcareous index nannofossils (coccoliths) of the lowermost Paleocene originated in the late Maastrichtian. Micropaleontology 49, 189–195. https://doi.org/10.2113/49.2.189

Martin, R.S., Witt, M.L.I., Sawyer, G.M., Thomas, H.E., Watt, S.F.L., Bagnato, E., Calabrese, S., Aiuppa, A., Delmelle, P., Pyle, D.M., Mather, T.A., 2012. Bioindication of volcanic mercury (Hg) deposition around Mt. Etna (Sicily). Chem. Geol. 310–311, 12–22. https://doi.org/10.1016/J.CHEMGEO.2012.03.022

Mason, R.P., Choi, A.L., Fitzgerald, W.F., Hammerschmidt, C.R., Lamborg, C.H., Soerensen, A.L., Sunderland, E.M., 2012. Mercury biogeochemical cycling in the ocean and policy implications. Environ. Res. 119, 101–117. https://doi.org/10.1016/J.ENVRES.2012.03.013

Möller, C., Bornemann, A., Mutterlose, J., 2020. Climate and paleoceanography controlled size variations of calcareous nannofossils during the Valanginian Weissert Event (Early Cretaceous). Mar. Micropaleontol. 157, 101875. https://doi.org/10.1016/j.marmicro.2020.101875

Moreno, T., Querol, X., Castillo, S., Alastuey, A., Cuevas, E., Herrmann, L., Mounkaila, M., Elvira, J., Gibbons, W., 2006. Geochemical variations in aeolian mineral particles from the Sahara-Sahel Dust Corridor. Chemosphere 65, 261–270. https://doi.org/10.1016/j.chemosphere.2006.02.052

Mulitza, S., Prange, M., Stuut, J.-B., Zabel, M., von Dobeneck, T., Itambi, A.C., Nizou, J., Schulz, M., Wefer, G., 2008. Sahel megadroughts triggered by glacial slowdowns of Atlantic meridional overturning. Paleoceanography 23, n/a-n/a. https://doi.org/10.1029/2008PA001637

Narciso, A., Cachão, M., De Abreu, L., 2006. Coccolithus pelagicus subsp. pelagicus versus Coccolithus pelagicus subsp. braarudii (Coccolithophore, Haptophyta): A proxy for surface subarctic Atlantic waters off Iberia during the last 200 kyr. Mar. Micropaleontol.

59, 15–34. https://doi.org/10.1016/j.marmicro.2005.12.001

Norris, R.D., Kroon, D., Klaus, A., 1998. Blake Nose paleoceanographic transect, western North Atlantic. Proc. ODP Init. Rep. B 171, 1–749. https://doi.org/10.2973/odp.proc.ir.171b.103.1998

O'Dea, S.A., Gibbs, S.J., Bown, P.R., Young, J.R., Poulton, A.J., Newsam, C., Wilson, P.A., 2014. Coccolithophore calcification response to past ocean acidification and climate change. Nat. Commun. 5, 1–7. https://doi.org/10.1038/ncomms6363

Ogg, J.G., Bardot, L., 2001. Aptian through Eocene magnetostratigraphic correlation of the Blake Nose Transect (Leg 171B), Florida continental margin. Proc. Ocean Drill. Program, Sci. Results B 171, 1–58.

Okada, H.; Bukry, D., 1980. Supplementary modification and introduction of code numbers to the low-latitude coccolith biostratigraphy (Bukry, 1973; 1975). Mar. Micropaleontol. 5, 321–325.

Petersen, S. V., Dutton, A., Lohmann, K.C., 2016. End-Cretaceous extinction in Antarctica linked to both Deccan volcanism and meteorite impact via climate change. Nat. Commun. 7, 12079. https://doi.org/10.1038/ncomms12079

Peterson, L.C., Haug, G.H., Hughen, K.A., Rohl, U., 2000. Rapid changes in the hydrologic cycle of the tropical Atlantic during the last glacial. Science (80-.). 290, 1947–1951. https://doi.org/10.1126/science.290.5498.1947

Pinet, P.R., Popenoe, P., 1985. A scenario of Mesozoic-Cenozoic ocean circulation over the Blake Plateau and its environs. Geol. Soc. Am. Bull. 96, 618–626. https://doi.org/10.1130/0016-7606(1985)96<618:ASOMOC>2.0.CO;2

Pyle, D.M., Mather, T.A., 2003. The importance of volcanic emissions for the global atmospheric mercury cycle. Atmos. Environ. 37, 5115–5124. https://doi.org/10.1016/J.ATMOSENV.2003.07.011

Quillévéré, F., Norris, R.D., Kroon, D., Wilson, P.A., 2008. Transient ocean warming and shifts in carbon reservoirs during the early Danian. Earth Planet. Sci. Lett. 265, 600–615. https://doi.org/10.1016/j.epsl.2007.10.040

Racki, G., 2021. “Big 5 Mass Extinctions.” Encyclopedia of Geology, 2nd ed. Academic Press. https://doi.org/10.1016/B978-0-12-409548-9.12028.7

Raffi, I., Backman, J., Zachos, J.C., Sluijs, A., 2009. The response of calcareous nannofossil assemblages to the Paleocene Eocene Thermal Maximum at the Walvis Ridge in the South Atlantic. Mar. Micropaleontol. 70, 201–212. https://doi.org/10.1016/j.marmicro.2008.12.005

Raffi, I., De Bernardi, B., 2008. Response of calcareous nannofossils to the Paleocene-Eocene Thermal Maximum: Observations on composition, preservation and calcification in sediments from ODP Site 1263 (Walvis Ridge - SW Atlantic). Mar. Micropaleontol. 69, 119–138. https://doi.org/10.1016/j.marmicro.2008.07.002

Ridgwell, A., Zeebe, R.E., 2005. The role of the global carbonate cycle in the regulation and evolution of the Earth system. Earth Planet. Sci. Lett. 234, 299–315. https://doi.org/10.1016/j.epsl.2005.03.006

Robock, A., 2000. Volcanic eruptions and climate. Rev. Geophys. 38, 191–219. https://doi.org/10.1029/1998RG000054

Rosenberg, Y.O., Ashckenazi-Polivoda, S., Abramovich, S., Thibault, N., Chin, S., Feinstein, S., Bartov, Y., Amrani, A., 2021. Resilience of primary and export productivity in a eutrophic ecosystem following the Cretaceous-Paleogene mass extinction. Glob. Planet. Change 196, 103371. https://doi.org/10.1016/j.gloplacha.2020.103371

Roth, P.H., 1994. Distribution of coccolith in oceanic sediments, Cambridge. ed, Coccolithophores. Cambridge Univ. Press, Cambridge.

Ruddiman, W.F., 2014. Earth’s Climate: past and future, 3rd ed. W. H. Freeman and Company, New York.

Sanei, H., Grasby, S.E., Beauchamp, B., 2012. Latest Permian mercury anomalies. Geology 40, 63–66. https://doi.org/10.1130/G32596.1

Scaife, J.D., Ruhl, M., Dickson, A.J., Mather, T.A., Jenkyns, H.C., Percival, L.M.E., Hesselbo, S.P., Cartwright, J., Eldrett, J.S., Bergman, S.C., Minisini, D., 2017. Sedimentary Mercury Enrichments as a Marker for Submarine Large Igneous Province Volcanism? Evidence

From the Mid-Cenomanian Event and Oceanic Anoxic Event 2 (Late Cretaceous). Geochemistry, Geophys. Geosystems 18, 4253–4275. https://doi.org/10.1002/2017GC007153

Schoene, B., Eddy, M.P., Keller, C.B., Samperton, K.M., 2021. An evaluation of Deccan Traps eruption rates using geochronologic data. Geochronology 3, 181–198. https://doi.org/10.5194/gchron-3-181-2021

Schoene, B., Eddy, M.P., Samperton, K.M., Keller, C.B., Keller, G., Adatte, T., Khadri, S.F.R.R., 2019. U-Pb constraints on pulsed eruption of the Deccan Traps across the end-Cretaceous mass extinction. Science (80-.). 363, 862–866. https://doi.org/10.1126/science.aau2422

Schueth, J.D., Bralower, T.J., Jiang, S., Patzkowsky, M.E., 2015. The role of regional survivor incumbency in the evolutionary recovery of calcareous nannoplankton from the Cretaceous/Paleogene (K/Pg) mass extinction. Paleobiology 41, 661–679. https://doi.org/10.1017/pab.2015.28

Sepkoski, J.J., 1996. Patterns of Phanerozoic Extinction: a Perspective from Global Data Bases. Glob. Events Event Stratigr. Phaneroz. 35–51. https://doi.org/10.1007/978-3-642-79634-0_4

Shen, J., Feng, Q., Algeo, T.J., Liu, Jinling, Zhou, C., Wei, W., Liu, Jiangsi, Them, T.R., Gill, B.C., Chen, J., 2020. Sedimentary host phases of mercury (Hg) and implications for use of Hg as a volcanic proxy. Earth Planet. Sci. Lett. 543, 116333. https://doi.org/10.1016/j.epsl.2020.116333

Shimabukuro, S., 1994. Braarudosphaera chalk": investigações sobre a gênese de um marco estratigráfico.["Braarusphaera chalk": investigation on the genesis of a stratigraphic mark]. M. Sc. Thesis Universidade Federal do Rio Grande do Sul.

Sprain, C.J., Renne, P.R., Vanderkluysen, L., Pande, K., Self, S., Mittal, T., 2019. The eruptive tempo of deccan volcanism in relation to the cretaceous-paleogene boundary. Science (80-.). 363, 866–870. https://doi.org/10.1126/science.aav1446

Thibault, N., Minoletti, F., Gardin, S., 2018. Offsets in the early Danian recovery phase in

carbon isotopes: Evidence from the biometrics and phylogeny of the Cruciplacolithus lineage. Rev. Micropaleontol. 61, 207–221. https://doi.org/10.1016/j.revmic.2018.09.002

Thierstein, H.R., Cortés, M.Y., Haidar, A.T., 2004. Plankton community behavior on ecological and evolutionary time-scales: when models confront evidence. Coccolithophores 455–479. https://doi.org/10.1007/978-3-662-06278-4_17

Watkins, D.K., Self-Trail, J.M., 2005. Calcareous nannofossil evidence for the existence of the Gulf Stream during the late Maastrichtian. Paleoceanography 20, 1–9. https://doi.org/10.1029/2004PA001121

Watson, A.J., 1997. Volcanic iron, CO2, ocean productivity and climate. Nature 385, 587–588. https://doi.org/10.1038/385587b0

Westerhold, T., Marwan, N., Drury, A.J., Liebrand, D., Agnini, C., Anagnostou, E., Barnet, J.S.K., Bohaty, S.M., De Vleeschouwer, D., Florindo, F., Frederichs, T., Hodell, D.A., Holbourn, A.E., Kroon, D., Lauretano, V., Littler, K., Lourens, L.J., Lyle, M., Pälike, H., Röhl, U., Tian, J., Wilkens, R.H., Wilson, P.A., Zachos, J.C., 2020. An astronomically dated record of Earth's climate and its predictability over the last 66 million years. Science (80-.). 369, 1383–1387. https://doi.org/10.1126/science.aba6853

Widmark, J.G.V., Speijer, R.P., 1997. Benthic foraminiferal ecomarker species of the terminal Cretaceous (late Maastrichtian) deep-sea Tethys. Mar. Micropaleontol. 31, 135–155. https://doi.org/10.1016/S0377-8398(97)00008-X

Winter, A.L., Jordan, R.W., Roth, P.H., 1994a. Biogeography of living coccolithophores in ocean waters.

Winter, A.L., Jordan, R.W., Roth, P.H., Svedarsky, W.D., 1994b. Biogeography of living coccolithophores in ocean waters.

Zachos, J.C., Arthur, M.A., Dean, W.E., 1989. Geochemical evidence for suppression of pelagic marine productivity at the Cretaceous/Tertiary boundary. Nature 337, 61–64. https://doi.org/10.1038/337061a0

Zachos, J.C., McCarren, H., Murphy, B., Röhl, U., Westerhold, T., 2010. Tempo and scale of late Paleocene and early Eocene carbon isotope cycles: Implications for the origin of

hyperthermals. Earth Planet. Sci. Lett. 299, 242–249.

https://doi.org/10.1016/j.epsl.2010.09.004

6. Appendix